ARL-SR-0459 ● JUNE 2022

2021 DEVCOM Army Research Laboratory Summer Student Program, Volume I: Symposium Presentations

Compiled by Danell Diggs

Approved for public release; distribution is unlimited.

NOTICES

Disclaimers

The findings in this report are not to be construed as an official Department of the Army position unless so designated by other authorized documents.

Citation of manufacturer's or trade names does not constitute an official endorsement or approval of the use thereof.

Destroy this report when it is no longer needed. Do not return it to the originator.

ARL-SR-0459 ● JUNE 2022



2021 DEVCOM Army Research Laboratory Summer Student Program, Volume I: Symposium Presentations

Compiled by Danell Diggs
Outreach Office, Plans and Programs, Laboratory Operations,
DEVCOM Army Research Laboratory

Approved for public release; distribution is unlimited.

REPORT DOCUMENTATION PAGE	Form Approved OMB No. 0704-0188

Public reporting burden for this collection of information is estimated to average 1 hour per response, including the time for reviewing instructions, searching existing data sources, gathering and maintaining the data needed, and completing and reviewing the collection information. Send comments regarding this burden estimate or any other aspect of this collection of information, including suggestions for reducing the burden, to Department of Defense, Washington Headquarters Services, Directorate for Information Operations and Reports (0704-0188), 1215 Jefferson Davis Highway, Suite 1204, Arlington, VA 22202-4302. Respondents should be aware that notwithstanding any other provision of law, no person shall be subject to any penalty for failing to comply with a collection of information if it does not display a currently valid OMB control number.
PLEASE DO NOT RETURN YOUR FORM TO THE ABOVE ADDRESS.

1. REPORT DATE *(DD-MM-YYYY)*	2. REPORT TYPE	3. DATES COVERED (From - To)
June 2022	Special Report	2021

4. TITLE AND SUBTITLE	5a. CONTRACT NUMBER
2021 DEVCOM Army Research Laboratory Summer Student Program, Volume I: Symposium Presentations	5b. GRANT NUMBER
	5c. PROGRAM ELEMENT NUMBER

6. AUTHOR(S)	5d. PROJECT NUMBER
Compiled by Danell Diggs	5e. TASK NUMBER
	5f. WORK UNIT NUMBER

7. PERFORMING ORGANIZATION NAME(S) AND ADDRESS(ES)	8. PERFORMING ORGANIZATION REPORT NUMBER
DEVCOM Army Research Laboratory ATTN: FCDD-RLL-D 2800 Powder Mill Rd Adelphi, MD 20783-1138	ARL-SR-0459

9. SPONSORING/MONITORING AGENCY NAME(S) AND ADDRESS(ES)	10. SPONSOR/MONITOR'S ACRONYM(S)
	11. SPONSOR/MONITOR'S REPORT NUMBER(S)

12. DISTRIBUTION/AVAILABILITY STATEMENT

Approved for public release; distribution is unlimited.

13. SUPPLEMENTARY NOTES

14. ABSTRACT

The US Army Combat Capabilities Development Command Army Research Laboratory Summer Student Symposium is a DEVCOM Army Research Laboratory Director's Award Program for all the students participating in various summer scholarship and contract activities across DEVCOM ARL. The goal of the program is to recognize and publicize exceptional achievements made by students and their mentors in support of Army science. All undergraduate and graduate interns were encouraged to submit an abstract summarizing their accomplishments and participate in the symposium, which was held on 12 August 2021. The posters presented are published in Volume I of the proceedings (this report), while abstracts are collected in Volume II (*Compendium of Abstracts*; ARL-SR-0460).

15. SUBJECT TERMS

DEVCOM ARL Summer Student Research, Summer Student Symposium, Student Outreach

16. SECURITY CLASSIFICATION OF:			17. LIMITATION OF ABSTRACT	18. NUMBER OF PAGES	19a. NAME OF RESPONSIBLE PERSON
a. REPORT	b. ABSTRACT	c. THIS PAGE			Danell Diggs
Unclassified	Unclassified	Unclassified	UU	45	19b. TELEPHONE NUMBER (Include area code) (301) 394-1092

Standard Form 298 (Rev. 8/98)
Prescribed by ANSI Std. Z39.18

Contents

Director's Foreword **iv**

1. Introduction **1**

2. 2021 DEVCOM ARL Summer Student Symposium Posters **2**

Distribution List **39**

Director's Foreword

The US Army Combat Capabilities Development Command Army Research Laboratory mission is to "operationalize science for transformational overmatch". As the Army's corporate research laboratory, we provide the technological underpinnings critical to providing capabilities required by the future Army.

In the coming years, our nation is projected to experience a shortage of scientists and engineers. Our laboratory recognizes the criticality of intellectual capital in generating future capabilities for the Army. It is critically important that we address the projected shortfall and make it a key responsibility of ours to close the impending gap. We have, therefore, identified the nation's next generation of scientists and engineers as a key community of interest, and have generated a robust educational outreach program to strengthen and support them. We have achieved many successes with this community. We believe that the breadth and depth of our outreach programs will have a significant and positive effect on the participants, facilitating their journey toward becoming our nation's next generation of scientists and engineers.

A fundamental component of our outreach program is to provide students research experiences at the DEVCOM Army Research Laboratory. During the summer of 2020, we supported research experiences at DEVCOM ARL for over 180 undergraduate and graduate students. Due to the COVID-19 pandemic, we were able to adapt and provide a highly effective virtual experience. As part of their experience, students present the results of the work they performed while at DEVCOM ARL. All of the presentations were of high quality, but only a few could be presented at our student symposium. The finalist presentations prepared this summer are contained in this volume of the proceedings, and they indicate that there were many excellent research projects with outstanding results. It is unfortunate that there was not enough time for us to have all of the presentations presented. We would have enjoyed hearing them all.

We are very pleased to have hosted this outstanding group of students for the summer. It is our hope that they will continue their pursuit of technical degrees and will someday assist us in providing critical scientific outcomes for our Army.

Patrick Baker
Director

1. Introduction

The US Army Combat Capabilities Development Command Army Research Laboratory Summer Student Symposium is a DEVCOM Army Research Laboratory Director's Award Program for students participating in various summer internship opportunities across DEVCOM ARL. The goal of the program is to recognize and publicize exceptional achievements made by the students and their mentors in the support of Army science.

All undergraduate and graduate interns are eligible to compete for a finalist position and give an oral presentation at the symposium. All students, including high school students in the Science and Engineering Apprentice Program (SEAP), are encouraged to present posters at the symposium and submit abstracts summarizing their accomplishments.

This year's symposium was held virtually on Thursday, 12 August 2021.

This volume of the Summer Student Symposium Proceedings contains the posters presented at the symposium. Volume II (ARL-SR-0460) is a compendium of student abstracts.

2. 2021 DEVCOM ARL Summer Student Symposium Posters

UNCLASSIFIED

AURORA Platform Static Application Security Testing

Clinton Anderson, Theron Trout, Mark Dennison

Overview

Project AURORA (Accelerated User Reasoning for Operations, Research, and Analysis), is being developed at the Army Research Lab (ARL), to enable effective collaboration between immersive and non immersive information systems across both tactical and command echelons. However, the valuable information exchanged within this framework demands an increased need to protect it. This research covers several black-box Software Application Security Testing ("fuzzing") tools and how they collaborate within AURORA's assorted networks, software, operating systems, game engines, and integrated development environments to create a secure fuzzing platform.

Background

Much of the data sent over tactical information systems cannot be sent over commercial networks, necessitating techniques in the lab for testing vulnerabilities in a secure, repeatable fashion.



A "fuzzer" is a Static Application Security Testing (SAST), or a Black Box, software testing technique that can find bugs in the software before deployment by injecting various data in an automated fashion. Operation and usage can vary based on operating system, programming language, hardware, type of fuzzing, etc.

Objective

- Provide a repeatable fuzzing framework that can be accomplished on Windows-specific dynamic linked libraries (.dll) and binaries (.exe).
- Explore which in-house fuzzing technique provides the best behavior, is easiest to use, and is most expandable.
- Create documentation on providing a testing platform, including creation of coverage modules and test harnesses.
- Research different continuous integration / continuous deployment (CI/CD) models that include Static (pre-deployment) and Dynamic (continuous deployment) security application tests.

Security Testing

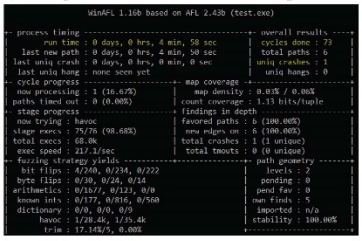
- AURORA is being developed on several operating systems: Windows 10, Linux
- Development is on multiple VR and AR platforms, such as HTC Vive, Oculus Quest 2, and Microsoft HoloLens2
- Off-line security fuzzers Peach and WinAFL were explored.
- Optimization tools were used, such as Ghidra, used to find specific addresses within AURORA code, and virtual environments, used to ensure specific requirements are met.

Observation

- Dll's and Exe's are Microsoft Windows based extensions. Many fuzzers only support Unix-based systems.
- Though Peach is standard in the fuzzing industry, much information on it is outdated since its acquisition by GitLab mid-2020—good documentation for it is spread among a plethora of sources, swapping between operating systems (32-bit vs. 64-bit, Windows vs. Unix), and uses the older 2.7 python version vs. current 3.8 randomly, making online troubleshooting difficult.
- Additionally, the Readme and Help documentation has ceased to be updated, and online forums provide answers from several years ago.
- This research will continue to incorporate this most-popular fuzzer, however, in the interest of maintainability and simplicity, other avenues should be concurrently pursued.

Method

- The Windows-based WinAFL is an expansion of the simpler alternative to Peach, the Linux based "AFL" (American Fuzzy LOP). This was found to be easier than Peach which had multiple errors on integration with modern software.
- As implementation progressed, additional applications such as CMake (used on older versions on Visual Studio), Ghidra (used to obtain address target offsets), and optimization methods like requirement-creation for virtual environments (to verify proper running on disparate machines) had to be incorporated.



Path Forward

- Develop easy-to-read documentation on how to install a fuzzer on a new machine, and how to create a harness, which is used to test specific functions in an optimized and more organized way.
- Explore continuous integration / continuous deployment (CI/CD) commercial environments such as Beyond Security's BeSECURE or GitLab DevSecOps.

Acknowledgments

• Dr. Mark Dennison, Mr. Theron Trout

NAVAL POSTGRADUATE SCHOOL

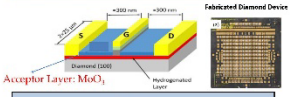
UNCLASSIFIED

ATOMISTIC STUDY OF PHASE-DEPENDENT STRUCTURAL AND ELECTRONIC PROPERTIES OF MOO_3

Researcher: Ms. Harsha Antony, University of California Riverside – DoD Researcher, hanto006@ucr.edu
Mentor: Dr. Mahesh Neupane, Research Scientist, ARL-WEST Los Angeles
U. S. Army Combat Capabilities Development Command Army Research Lab

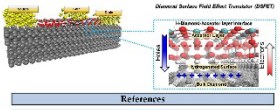
Introduction

- Surface-doped diamond devices utilize charge transfer mechanism between acceptor layer (MoO_3, WO_3 and V_2O_5) and hydrogen-terminated diamond surface



Objectives

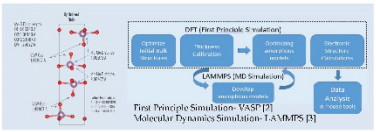
- Developing amorphous models of MoO_3
- Analyze structural and electronic properties amorphous MoO_3
- Design MoO_3/H-Diamond Heterostructure
- Analyze charge transfer across the interface



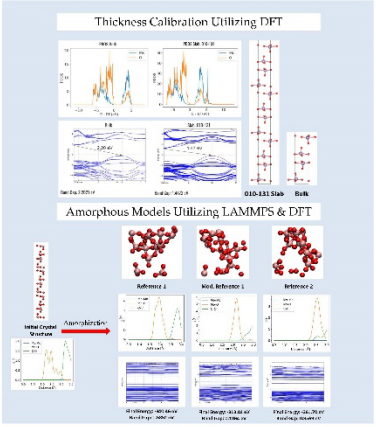
References

1. [illegible]
2. G. Kresse and J. Hafner, Phys. Rev. B 47, 558 (1993); ibid. 49, 14 251 (1994).
3. A. P. Thompson, H. M. Aktulga, R. Berger, D. S. Bolintineanu, W. M. Brown, P. S. Crozier, P. J. in 't Veld, A. Kohlmeyer, S. G. Moore, T. D. Nguyen, R. Shan, M. J. Stevens, J. Tranchida, C. Trott, and S. J. Plimpton, Comp. Phys. Comm. 271, 108171 (2022).
4. J. Wiercigroch, K. E. Byrne, A. Szlapa-Kula, M. Malicka, J. C. Walczak, S. M. Kastrup, M. Gajewska, A. Kula, and B. Cyranski, Spectrochim. Acta A Mol. Biomol. Spectrosc. 227, 117640 (2020).
5. Gonzalez, Rafael I. (2020). Ashby's Virtual Process Methodology for Material Selection. Doctoral Thesis, University of Kent.

Model and Methods



Results



Observations

- For Molecular Dynamics Simulations utilizing LAMMPS, there is no available potential force field to model amorphous MoO_3 for us, thus it require development of a new force field.
- Thus, we have modified available force fields (developed for other Mo-O complexes and for crystalline MoO_3) and designed amorphous models

Conclusion

- We did calibration of Layer Thickness in DFT utilizing VASP to observe Bulk like structural and electronic properties
- The results include Binding Energy, Band alignment, Densities of states, Work function
- Validated parameters for a simple 2 body potential force field for amorphous models
- Refined melt-quench process to generate amorphous models

Pathway Forward

- Fully develop LAMMPS potential, accurately model amorphous MoO_3, and validate generate models with experimental data
- Validate force fields and models with more established force field from Dr. Vashishta (USC)
- Use developed amorphous models and design heterostructures with diamond to analyze surface charge transfer between the amorphous MoO_3 and the diamond and guide in-house experimental effort

Acknowledgements

- DOD HBCU/MI Summer Research Program
- U.S. Army Combat Capabilities Development Command Army Research Lab
- Dr. Alex Greaney and Pegah Mirabedini, Computational Materials Science Lab, UCR

U.S. ARMY COMBAT CAPABILITIES DEVELOPMENT COMMAND – ARMY RESEARCH LABORATORY

Mohammed Safayet Arefin

PhD Candidate

Computer Science and Engineering

Mississippi State University, USA

Advisor: Dr. J. Edward Swan II



Research Interest

Augmented Reality, Applied Perception, Virtual Reality, Visual Perception

UNCLASSIFIED//FOR OFFICIAL USE ONLY//DRAFT//PRE-DECISIONAL

UNCLASSIFIED//FOR OFFICIAL USE ONLY//DRAFT//PRE-DECISIONAL

Tracking Perceptual Depth with Eye Vergence and Inter Pupillary Distance in VR

Summer Intern

CCDC US Army Research Laboratory (ARL-WEST)

Dr. Russell A. Cohen Hoffing



Adviser

Dr. Steven Thurman



Virtual Reality







- VR is an emerging technology with multiple potential use cases in Army.
- Simulated complex training environment.
- Platform for common operating picture.
- For conducting basic research.



Eye Tracking

- Better understanding of how our human visual system behaves.
- Eye behaviors provides important signal of the cognitive processes.
  - Opportunistic sensing systems use eye activity to adapt to the user and improve mission performance.



Eye Tracking +VR

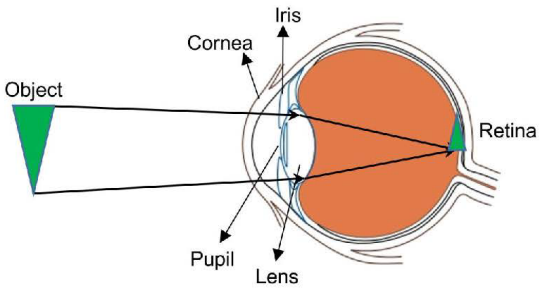
- VR with integrated Eye Tracking Technology newer technology.
- Could be used to improve the accuracy of size and distance cues in the simulated scene. Unexplored research area.
- **Can eye tracking parameters be related to depth in VR?**



Image Source: Images are taken from Internet

Human Visual System

Human Eye



Accommodation

• The ability of the eye to adjust its focal length is known as ***accommodation***.

[Gross, H., Blechinger, F., and Achtner, B. 2015. Human Eye. John Wiley & Sons, Ltd.]

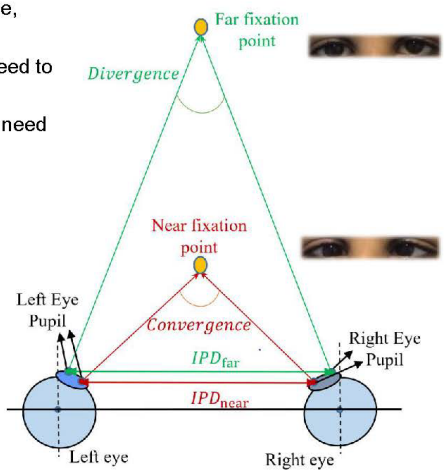
Human Visual System

Vergence

- Viewing object at different distances requires the eyes to rotate, which is known as ***vergence***
- When **shifting gaze from far to a nearby object**, the eyes need to rotate inward, which is known as ***convergence***
- When **shifting gaze from near to a distant object**, the eyes need to rotate outward, which is known as ***divergence***.

The value of vergence angle is larger during convergence than divergence

Vergence-Accommodation Reflex



Inter Pupillary Distance (IPD)

- Distance between the center of left eye's pupil to the center of right eye's pupil
  - **During convergence, IPD becomes smaller**
  - **During divergence IPD becomes larger**

[Gross, H., Blechinger, F., and Achtner, B. 2015. Human Eye. John Wiley & Sons, Ltd.]

Experiment

Research Goal

Tracking Perceptual Depth with Eye Vergence and Inter Pupillary Distance in VR

A visual discrimination task with unrestricted eye and head movement

HTC Vive VR headset with Eye tracking from Tobii Technologies

24 subjects

Counterbalanced **288 trials**

Perceptual Depth

Near (13m) and far (32m)

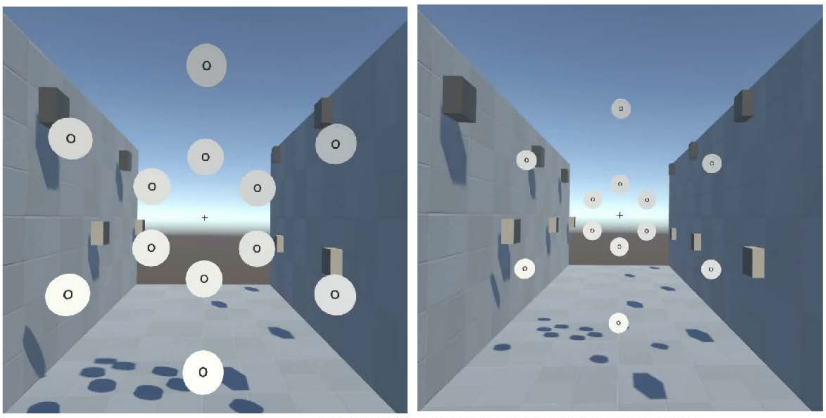
Virtual Object Position

Parafovea and Periphery

Data Collection

US Air Force Academy (AFA)

Dr. Anothony Ries and colleagues



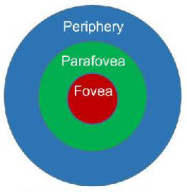
Perceptually virtual Disks are closer than the recentering cross

How can we measure vergence and IPD from the eye tracker data in VR?

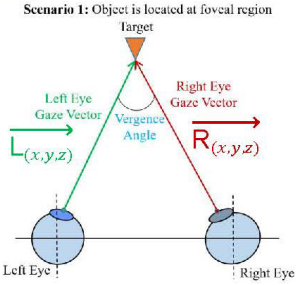
UNCLASSIFIED//FOR OFFICIAL USE ONLY//DRAFT//PRE-DECISIONAL

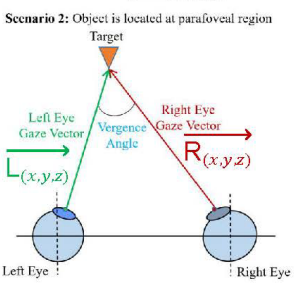
Vergence Calculation

In this experiment **targets are presented at the parafovea and periphery location**



Macula of Retina





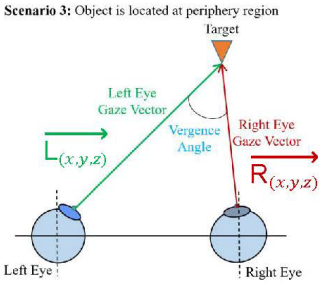
Calculated Vergence angle by using **3D Gaze Direction Unit Vector**

Left and right eye gaze direction vector $\overrightarrow{L_{(x,y,z)}}$ and $\overrightarrow{R_{(x,y,z)}}$

Therefore, according to the **vector dot products**,

$$\overrightarrow{L_{(x,y,z)}} \cdot \overrightarrow{R_{(x,y,z)}} = L \times R \cos\theta$$

$$\text{Vergence angle, } \theta = \cos^{-1} \frac{\overrightarrow{L_{(x,y,z)}} \cdot \overrightarrow{R_{(x,y,z)}}}{L \times R}$$



Sulutvedt, Unni & Mannix, Thea & Laeng, Bruno. (2018). Gaze and the Eye Pupil Adjust to Imagined Size and Distance. Cognitive Science. 42. 10.1111/cogs.12684.

Inter Pupillary Distance (IPD) Calculation

Distance between the center of left eye's pupil to the center of right eye's pupil

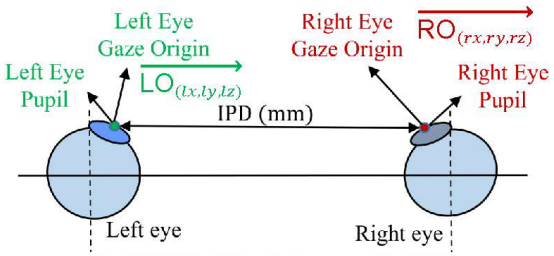
Calculated IPD by considering **3D Gaze Origin Vector**

Tobii Pro SDK provides gaze origin vectors to indicate the center of the pupil position
Source: https://developer.tobii.com/product-integration/stream-engine/#tobii_streamsh

Left and right eye gaze origin vector, $\overrightarrow{LO_{(lx,ly,lz)}}$ and $\overrightarrow{RO_{(rx,ry,rz)}}$

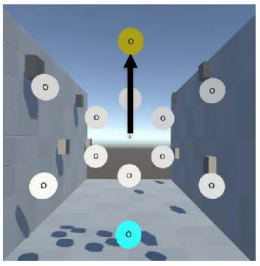
Therefore, according to the **Euclidian distance formula**,

$$\text{IPD} = \sqrt{(lx - rx)^2 + (ly - ry)^2 + (lz - rz)^2}$$



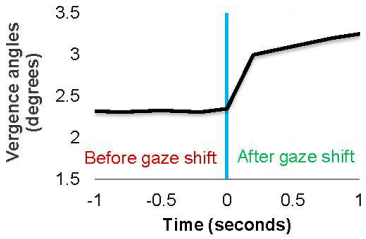
Hypothesis

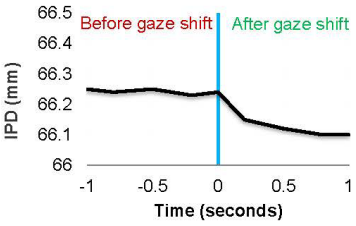
Shifting eye gaze from the cross to the virtual disk



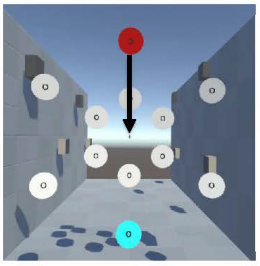
Convergence

First saccade onset after cue is presented (Blue Vertical Line)



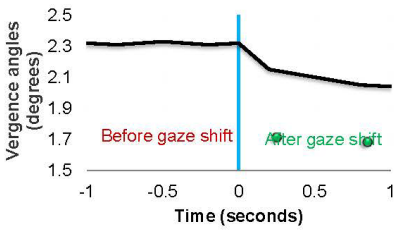


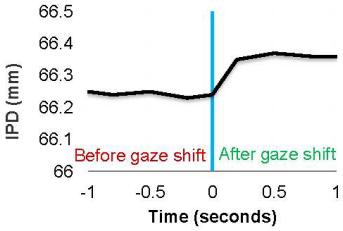
Shifting eye gaze from the virtual disk to the cross



Divergence

First saccade onset after target is deactivated (Blue Vertical Line)

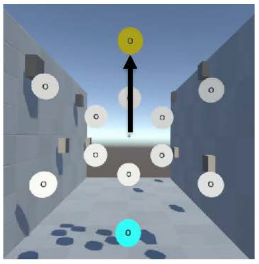




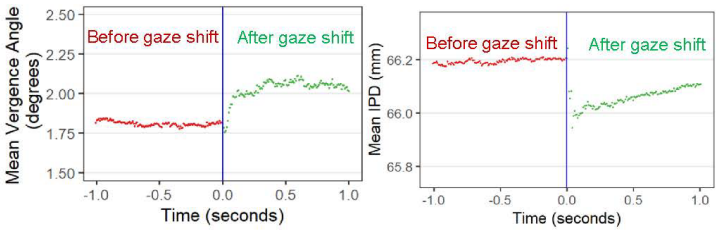
Results

Convergence

Shifting eye gaze from the cross to the virtual disk

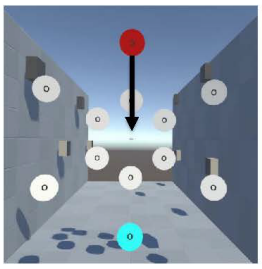


First saccade onset after cue is presented (Blue Vertical Line)

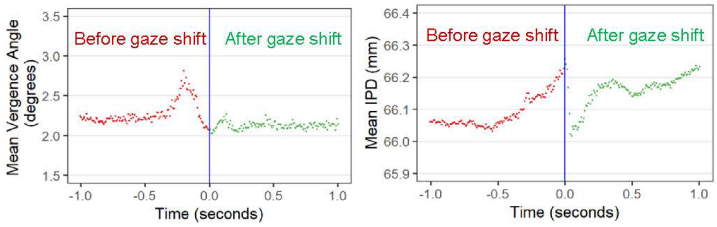


Divergence

Shifting eye gaze from the virtual disk to the cross



First saccade onset after target is deactivated (Blue Vertical Line)

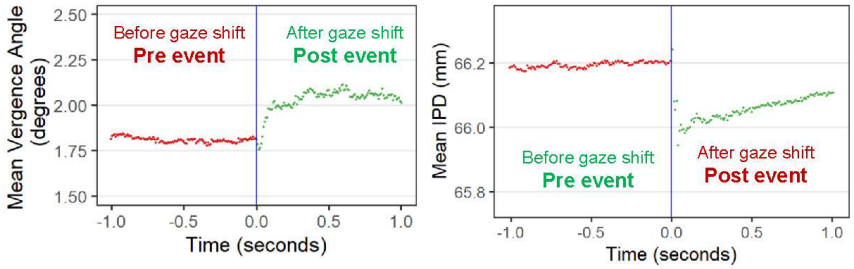


Results

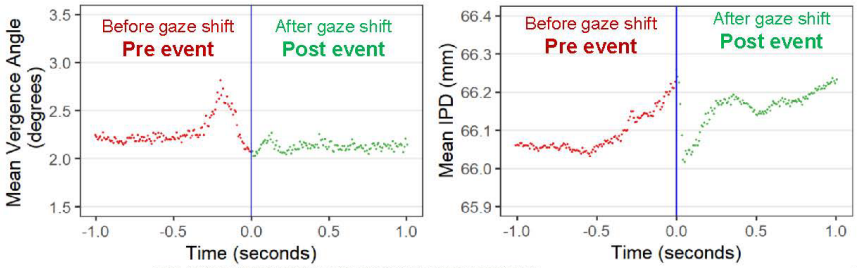
Amount of vergence angle and IPD changes between before and after the gaze shift

Amount of changes = Post event (+1 seconds) – Pre event (-1 seconds)

Convergence



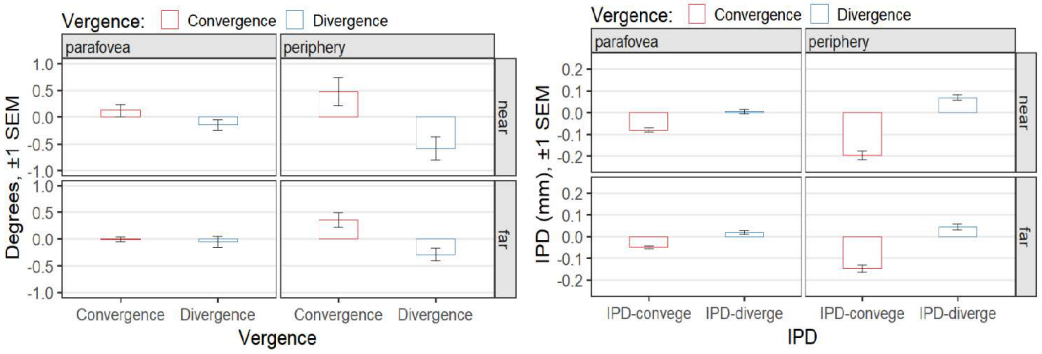
Divergence



Results

Amount of vergence angle and IPD changes between before and after the gaze shift

Amount of changes = Post event (+1 seconds) – Pre event (-1 seconds)

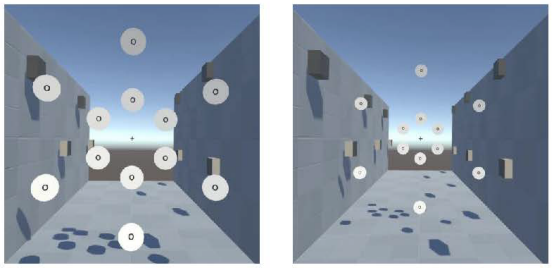


Repeated Measures (2 x 2 x 2) ANOVA Analysis

- Significant main effect for vergence movements both measures (vergence angle, IPD).
- Significant interaction effect with target position such that both measures have larger changes comparing periphery to parafovea; means periphery perceptually observed much closer.
- Significant interaction effect with target depth for IPD measures which means that near target was indeed perceived closer.

Conclusion

- We can objectively track perceptual depth with eye vergence and IPD measures derived from the eye tracking data.
  - IPD appeared to be more robust measures than vergence angle
- Next steps:
  - Design a more controlled study with ground truth to assess the precision and accuracy of the measurement in VR for tracking perceptual depth.
  - Writing and publishing the paper.
  - Future Application:
    - Adaptively rendering virtual objects at the perceptual depth plane.
    - Evaluate ways to improve user experience in VR

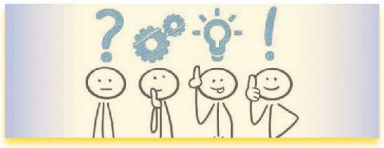


Special Thanks

DEVCOM ARMY RESEARCH LABORATORY

ARL WEST

Discussion & Questions

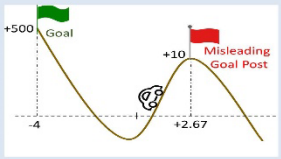


Approximate Persistent Exploration in Reinforcement Learning over Continuous Spaces

Amrit S. Bedi and Alec Koppel
CISD, ARL

Motivation

- Reinforcement Learning (RL) in continuous control task
- Learning a Q function in continuous space is not possible
- Monte Carlo Tree search or Bellman's equations doesn't work
- We focus on **Policy Gradient** (PG) methods
- Challenge: RL is nonconvex and rewards could be sparse
- Results in spurious behavior for standard learning procedure
- Recently, non-asymptotic guarantees to local optimal $\mathcal{O}(1/\epsilon^2)$
- Any stronger notion possible? (like global optimality in tabular)
- Key intuition is **persistent exploration** in tabular settings
- Goal: Can one avoid convergence to spurious local minima in MDPs over continuous spaces through appropriate policy parameterizations?
- Example: Pathological Mountain Car



Problem Formulation

- Consider the MDP $\mathcal{S}, \mathcal{A}, \mathbb{P}, r, \gamma$
- Value function

$$V^{\pi}(s) = \mathbb{E}\left[\sum_{t=0}^{\infty} \gamma^t r(s_t, a_t) \mid s_0 = s, \pi\right]$$

- Policy search over policies $\pi_\theta(\cdot|s_t)$
- Maximize the expected cumulative return

$$\max_{\theta} J(\theta) := V^{\pi_\theta}(s_0)$$

- Nonconvex optimization problem
- Example: Gaussian Policy

$$\pi_\theta(a|s) = \mathcal{N}(a|\phi(s)^\top \mathbf{x}, e^y)$$

Proposed Algorithm

Algorithm 1 Heavy-tailed Policy Gradient (HPG)

1: **Initialize** : policy parameters $\boldsymbol{\theta}_0$, discount γ, step-size η, gradient $\mathbf{g}_0 = \mathbf{0}$, starting point (s_0, a_0)
Repeat for $k = 1, \ldots$
2: Starting from (s_0, a_0) , generate B_k trajectories $\tau_{k,i} = (s_0, a_0, s_1, a_1, \ldots s_{T_{k,i}}, a_{T_{k,i}})$ of length $T_{k,i} \sim \text{Geom}(1-\gamma^{1/2})$ with actions $a_u \sim \pi_{\boldsymbol{\theta}_k}(.|s_u)$
3: Compute policy gradient estimate $\mathbf{g}_k$ and update parameters $\boldsymbol{\theta}_k$:

$$\mathbf{g}_k \leftarrow \frac{1}{B_k}\sum_{i=0}^{B_k}\left[\sum_{t=0}^{T_{k,i}} \gamma^{t/2} \cdot R(s_t, a_t) \cdot \left(\sum_{\tau=0}^{t} \nabla \log \pi_{\boldsymbol{\theta}_k}(a_\tau \,|\, s_\tau)\right)\right],$$

4: $k \leftarrow k+1$ **Until Convergence**
5: **Return:** $\boldsymbol{\theta}_k$

Convergence Results

- Gradient norm attenuation rate

$$\frac{1}{K}\sum_{k=0}^{K-1}\mathbb{E}\left[\|\nabla J(\theta_k)\|_2^2\right] \leq \frac{a_\beta}{K^{\frac{\beta}{1+\beta}}} + \mathcal{O}(\lambda)$$

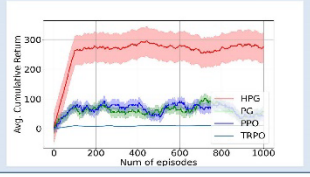
- Metastability (Transition time)

$$\lim_{\epsilon \to 0} \quad \mathcal{P}^{\theta_0}(\theta^k \in \Omega_i^+(\bar{\delta}) \cap \partial\mathcal{G}_{i+1}) \geq \frac{d_{ij}^{-\alpha}}{((d_{ij}^+)^{-\alpha} + (-d_{ij}^-)^{-\alpha}} - \delta$$

- HPG converges to "wider" peaks
- Nearly satisfy persistent exploration in MDPs over continuous spaces

Experiments

- Proof of concept experiments with Cauchy policy



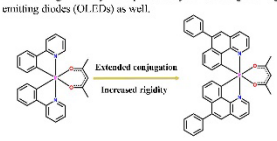
APPROVED FOR PUBLIC RELEASE

Retrosynthesis of Benzoquinoline Derivative Ligands for Cyclometalated Iridium Complexes

Student: Evan Bolster, *ebolster001@csbsju.edu*
Mentors: Ryan O'Donnell & TJ Rohrabaugh
ryan.m.odonnell.civ@mail.mil; thomas.n.rohrabaugh.civ@mail.mil

Overview

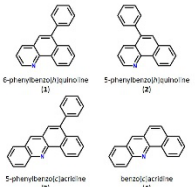
Cyclometalating iridium (III) complexes containing acetylacetonate and two fairly conjugated ligands, such as 2-phenylpyridine, exhibit a strong, temporary absorption of visible light following photoexcitation. This process is called reverse saturable absorption (RSA) and is currently investigated by the Army Research Laboratory. Cyclometalated iridium complexes typically exhibit excited state lifetimes on the order of hundreds of nanoseconds to microseconds before returning to the ground state. *Our goal is to improve the photophysics of these complexes, by designing materials with excited state lifetimes on the order of hundreds of microseconds to milliseconds.* These types of materials would be advantageous for RSA applications and more generically for photocatalysis and organic light emitting diodes (OLEDs) as well.



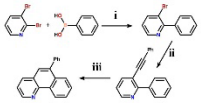
Commonly, extending aromatic conjugation or manipulation of electron donating or electron withdrawing functional groups are investigated as a way to enhance excited state lifetimes. **This research identified and performed a retrosynthetic analysis of four different benzoquinoline-based ligands which had potential to improve the excited state.** All four of these compounds would employ Suzuki-Coupling reactions to create carbon-carbon bonds between a pyridine and a phenyl ring. Two molecules would then use a Sonogashira-Coupling reaction to create a terminal alkyne on the 2-carbon of the pyridine or phenyl. The other two molecules would create the alkyne from an aldehyde using a Bestmann-Ohira reaction. Finally, all four molecules would be treated with triflic acid to induce cycloisomerization and the formation of the benzoquinoline ring. **It is predicted that extending the conjugation of these ligands and enhancing their rigidity, especially between the iridium bonded carbon and nitrogen, should dramatically increase the duration of the complex's excited state.** Furthermore, ligand positions for further derivatization with electron donating or electron withdrawing functional groups were identified.

Materials and Methods

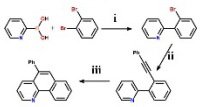
Target Molecules



Pathway for 1



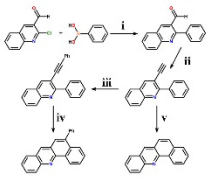
Pathway for 2



Conditions for 1 & 2:

i. $Pd(OAc)_2$ (5 mol%), PPh_3 (10 mol%), K_2CO_3, MeCN/MeOH (2:1), 50°C, 24 hrs
ii. Phenylacetylene, $Pd(PPh_3)_2Cl_2$ (5 mol%), CuI (5 mol%), DMA, Et_3N, 90°C, 6 hrs
iii. TfOH, 15 min, rt

Pathway for 3 & 4



Conditions for 3 & 4:

i. - $Pd(PPh_3)_4$ (5 mol%), K_2CO_3, DMA/Water (1:1), 120°C, 3 hrs
ii. Bestmann-Ohira Reagent (1-diazo-2-oxo propylphosphonate), K_2CO_3, MeOH, rt, 12 hrs
iii. PhI, Et_3N, $Pd(PPh_3)_2Cl_2$ (5 mol%), CuI (5 mol%), MeCN, 80°C, 6 hrs
iv. TfOH, 1 hr, rt
v. $PtCl_2$ (10 mol%), PhMe, 120°C, 20 hrs

Expected Results

Estimated progressive yields based on literature from starting compounds to target molecules are very reasonable for 3-1 step syntheses: **1)** 61% **2)** 73% **3)** 38% **4)** 28%.

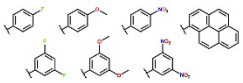
The starting materials also have relatively cheap small scale prices making them ideal for testing: **1)** $55.63/g **2)** $35.19/g **3)** $31.06/g **4)** $55.50/g

After successful synthesis, the target molecules will be used to synthesis the corresponding iridium complex and photophysical properties investigate

APPROVED FOR PUBLIC RELEASE

Future Work

The ligands can be further modified with different phenyl derivatives by substituting a variety of different phenylacetylenes in step ii for molecules **1** and **2**, or different aryl halides in step iii for molecule **3**



References

[1] Shestakov, A.; Pankova, A.; Kuzmitsov, M. Cycloisomerization – a straightforward way to benzo[h]quinolines and benzo[c]acridines. *Chemistry of Heterocyclic Compounds* **2017**, *53* (10), 1103–1113. DOI: https://doi-org.ezproxy.csbsju.edu/10.1007/s10593-017-2179-5

[2] Qizhong, Z.; Bin, Z.; Liangjun, S.; Tiansheng, L.; Renze, C.; Tieqi, D.; Yayuan, Y.; Jianfen, S.; Guoliang, D.; Deman, H.; Huajiang, J. Palladium-catalyzed highly regioselective 2-arylation of 2,x-difluoropyridines and its application in the efficient synthesis of a LTβ4H5DI inhibitor. *Tetrahedron* **2013**, *69* (51), 10996-11003. DOI: https://doi.org/10.1016/j.tet.2013.10.065.

Evan Bolster would like to thank Dr. Ryan M. O'Donnell and Dr. Thomas N. Rohrabaugh, Jr. *U.S. Army DEVCOM ARL SEDD* for their mentorship

Evan Bolster would like to acknowledge funding from The U.S. Army Cadet Command that supported his ARL-ROTC summer internship

Mentor: Dr. Julia Wright
Intern: Giovanna Camacho

Can't We Just Agree with the HAT? Agreeableness in Human Agent Teaming

Background

Part of the DOD's modernization initiative is the Next Generation Combat Vehicle (NGCV) program. This program specifically focuses on requirements such as: being optionally manned, operating remotely, and utilizing artificial intelligence with certain tasks to assist crewmembers. Part of being successful in this initiative is reconciling both where the Human Autonomy Teaming (HAT) falls short and what actions can be taken to enhance their effectiveness. Recent advancements in artificial intelligence and machine learning have enabled the creation of learning capable agents (LCAs). Although humans teaming with autonomy has been relatively well researched, little is known how teaming with LCAs will influence that human teammate.

Human Autonomy Teaming and Personality Influence

HAT has been shown to support the human's performance on subsequent tasks. However, these performance outcomes are influenced by the operators individual differences in areas such as spatial ability, attentional control, etc. One individual difference factor that has not been researched extensively in HAT is personality, or the 'Big Five'. Understanding how the operators' personality can influence their performance outcomes in HATs can be helpful in the development of autonomy that better supports their human teammate.

Why focus on agreeableness?

Individuals who are high in agreeableness are helpful, cooperative, get along well with others, and develop strong relationships with team mates. As such, individuals high in agreeableness can be expected to perform well in HATs. All participants in this study scored above average on the Agreeableness measure (>3 out of 5), so we examined how subtle differences in agreeableness affect task outcomes.

Hypothesis

There will be differential effects in HAT outcomes due to individual differences in agreeableness.

Experimental Design

This 2 (reasoning transparency: opaque vs. transparent) x 3 (learning transparency: implicit, explicit, human-directed) fractional factorial within-subjects study assesses the effects of transparency of agent reasoning and learning on a threat classification task.

		Learning		
		Implicit	Explicit	Human-Directed
Reasoning	Opaque	T1	---	---
	Transparent	T2	T3	T4

- **Opaque Reasoning/Implicit Learning (T1)**, agent conducts task without sharing reasoning or learning
- **Transparent Reasoning/Implicit Learning (T2)**, agent shares its reasoning but does not explicitly learn the participant's inputs used to learn.
- **Transparent Reasoning/Explicit Learning (T3)** agent shares its reasoning and explicitly learning information based upon participant input
- **Human Directed Learning (T4)** agent shares its reasoning, and the participant completes any missing learning information before identifying a potential threat

Equipment

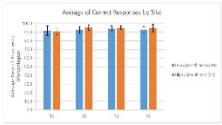


Figure 1: Example left monitor showing map of the area, planned route, command communication modules, and route comparator.

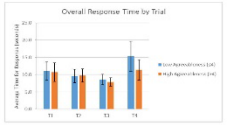
Figure 2: Example right monitor showing mission brief, threat classification, and agent's Status Bar.

The left monitor showed the route comparator, an overhead view map of the simulation environment, and a text display for "commander messages" (Figure 1). The right monitor shows the simulated environment surrounding the NGCV, the agent's reasoning for each person they encountered, and buttons relevant to the class Hazelton task (Figure 2).

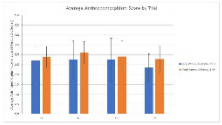
Results



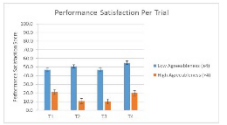
Graph 1: There was no difference in the percent of correct identification between the two agreeableness groups, except when agent reasoning was transparent and learning was explicit (F, p = .149, δ_p = .12).



Graph 2: Regardless of their innate attributes of agreeableness, participants had faster response times as transparency increased, until the human directed condition, where the lower agreeableness participants were significantly slower than their higher agreeableness counterparts (F, p = .027, δ_p = .106).



Graph 3: Anthropomorphic ratings were slightly higher in participants who rated higher in agreeableness (F, p = .169, δ_p = .03).



Graph 4: Individuals who were higher in agreeableness had greater performance satisfaction than their lower agreeableness counterparts in all transparency conditions (F, p = .024, δ_p = .12; F, p = .04, δ_p = .10; F, p = .049, δ_p = .09; F, p = .006, δ_p = .15).

Higher agreeableness participants had the most performance satisfaction in the conditions where reasoning and learning were transparent (T2 & T3) than in the opaque condition (T1) or the human-directed learning condition (T4).

Methods & Surveys

Participants, Apparatus, and Task

Twenty participants were compensated 30 USD per hour. Participants used a desktop computer running an Unreal-based simulation of an urban environment. The computer setup consisted of two 15" monitors (1680 x 1050 resolution), standard wireless keyboard, and three button mouse (Figures 1 and 2).

Participants teamed with a simulated AI/R agent to conduct a threat classification task. They monitored their surroundings as their vehicle progressed through the environment. They completed 4 trials, 1 in each condition. The following surveys were completed by the participants.

Personality: The mini-IPIP (Donnellan, Oswald, Baird, & Lucas 2006) was used to assess an individual's personality across 5 distinct factors. The survey's scoring range is 1 – 5, with lower scores indicating less of a factor. In this study, all participants were high agreeableness (scores >3). The median range of scores was 4, so median split was used to divide into less prosocial (lower agreeableness mid-4 and higher agreeableness mid-5).

Workload: The NASA-TLX (Hart & Staveland, 1988) was used to assess perceived cognitive workload across 6 factors.

Anthropomorphic Tendencies: The Godspeed Questionnaire Series (GQS) consists of 21 questions based around five factors that determine a humans' perception of an agent. (Bartneck, Kulic Croft & Zoghbi, 2008).

Discussion

In performance outcome there was little difference between the higher and lower agreeableness individuals as the transparency conditions increased. However, when the participants were responsible for directly teaming the agent, response times increased and anthropomorphic evaluations decreased. The small difference in agreeableness between the two groups seemed to be these effects for some individuals. The higher agreeableness appeared to manifest in increased openness to work with an agent, as was evident in the subjective anthropomorphic ratings, as well as the greater performance satisfaction ratings.

Conclusion

Agreeableness, as a personality trait, can be a desirable trait in many team members, as it frees teams results, it appears the same holds true for persons in HATs that include LCAs. While there was slight benefits for performance outcomes and learning attitudes due to increased transparency, higher agreeableness seemed to hamper the added difficulty of instructing the agent. Further research could examine ways to support individuals' innate agreeableness when teaming with LCAs.

Acknowledgements

Dear Sara was by Dr. Julia Wright, Dr. Albert Jacobs, Dr. Anthony Kelmann, Dr. Jessica D. Collins, Mr. Jamie Wilson, Mr. Joseph Alexander, Ms. Johnna Swan, and the Army Research Laboratory for fostering such an opportunity and providing support, guidance, and learning.

CATALYTIC NANOTHERMOMETERS: NEW TEMPERATURE MODEL IN THEORY AND PRACTICE

Carroll, Alison L.
Mentors: Dr. Baker, Dr. Boltersdorf, Dr. Forcherio (NSWC), Dr. Diaz (NRL)

Abstract

Photocatalysis is a growing field of research within the scientific community due to its intriguing use of heat production in materials using light, which could be an asset to the Army's chemical needs. Much research has been done exploring the relationship between thermal and optical properties of nanoscale materials, most notably gold, yet there is a gap in understanding between theoretical and experimental results. This research project aims to better understand this relationship using nanothermometers made of DNA and gold. This will allow additional photocatalysts of interest, transition metal nitrides like TiN, to be explored with a new temperature model. Optical properties observed in the lab will be compared to those seen using DDSCAT, a dipole approximation program. From here, the nanothermometers will be examined when heated using fluorescent signalling and an absorbance/temperature model can be proposed. This new model will open the door for an improved, more cost efficient, and comprehensive photocatalytic process for the Army.

Classical Temperature Model

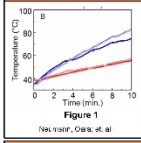


Figure 1

Neumann, Oara, et. al

$$\Delta T(R_{NP}) = \frac{V_{NP} P_{abs}}{4\pi k_0 R_{NP}}$$

This model is widely accepted by the field for NP heat generation when hit with incident light, but falls short of explaining observed heating behaviors and predicting realistic temperature changes at NP surfaces

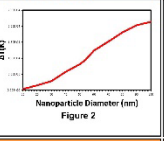


Figure 2

Nanothermometer Function and Signaling

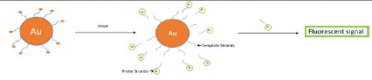


Figure 9

When heated, the probe strands will dissociate and release fluorescent signals that will be picked up by the fluorimeter. This signal will then be interpreted to represent the amount of probe strands that have detached from the nanoparticle, and thus give a temperature value of the nanoparticle.

DDSCAT and Simulated Optical Properties

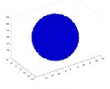


Figure 3

Visual representation of shape composed of dipoles from DDSCAT

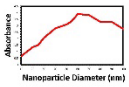


Figure 4

Ideal size Au nanosphere determination based on maximum absorbance

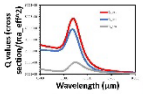


Figure 5

Optical properties of 60 nm diameter Au sphere

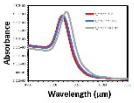


Figure 6

Absorbance values for blank AuNP, 9 nm DNA and 14 nm DNA attachments onto AuNP

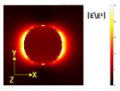


Figure 7

Nearfield map for blank 60 nm AuNP ran through DDSCAT and DDPOSTPROCESS

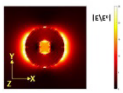


Figure 8

Nearfield map for 60 nm AuNP with 9 nm DNA shell

Needs additional modifications in MatLab code

Nanothermometer Synthesis

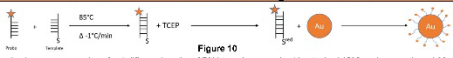


Figure 10

This synthesis process was done for 4 different lengths of DNA templates, each with attached 45°C probe strands and 60 nm diameter Au nanospheres. The nanothermometers underwent extensive washing and centrifugation steps to ensure the removal of unattached or single-stranded DNA that may have remained from the earlier synthesis steps.

TEM and In-Lab/ Simulated Data Comparisons

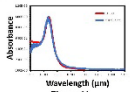


Figure 11

Simulated absorbance values from DDSCAT for blank 60 nm AuNP and diluted 1:10 AuNP suspended in solution measured by UV-Vis spectroscopy

TEM images of 60 nm AuNP bar bulk

Plan to get TEM images of synthesized dsDNA-AuNP nanothermometers



Figure 12

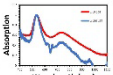


Figure 13

Serial Dilutions of ~ 5T nano thermometers show new peaks in the 750 nm range

Nanothermometers will go through a series of heating tests to examine fluorescent signaling. Temperature data will be paired and interpreted with optical properties observed and predicted with UV-Vis and DDSCAT data

TiN and Looking Forward

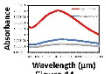


Figure 14

Interesting a varying optical properties when compared to Au: broader peaks

Visible extra layer of energy enhancement with added DNA



Figure 15



Figure 16



Figure 17

SELF-RIGHTING ROBOTICS ON VARYING LANDSCAPES

Pascal Conroy, ARL-CISD

Overview

Army Objective:
Advance self-righting capability for robotic platforms in rough terrain.

Research Goal:
Improve performance of robotic self-righting algorithms in rough terrain.

Research Needs:
A way to develop and test simulated robotic platforms on a landscape made up of varying height points.

Method:
Generating simulated variable terrain, and automatically testing the effect on self-righting performance within the LIMMBS Manipulation Team's PyBullet simulator.

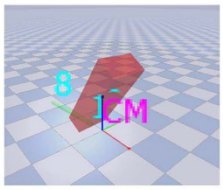


Figure 1. 1 DOF robot in one iteration for checking stable states. A stable state is tested by checking if the center of mass (CM in magenta) is within the face parallel and closest to the ground.

Current Abilities

- Intake mesh-based robot via URDF file
- Sample joint space of robot
- Evaluate stability of robot at varying poses per joint sample on flat ground
- Create stability graph for self-righting

Background

UGVs in use by the Warfighter must be able to travel wherever the warfighter can go, along with places they cannot, at the speed of the fight. They must also have hardware and software that is robust to the battlefield environment. Currently, a few commercially available robotic platforms are equipped with self-righting capabilities, but even those can only achieve this goal on simple, relatively level terrain.

The ability to recover robustly from tip-over (i.e. self-right) on rough terrain is vital to enabling travel at high speed by making the risks of tip-over tolerable. Ultimately, this capability will facilitate the expanded integration of robotics and autonomous systems for the military.

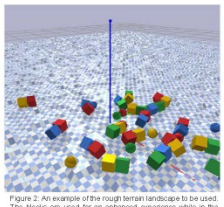


Figure 2: An example of the rough terrain landscape to be used. The blocks are used for an enhanced experience while in the live simulator, but are ancillary to the end goal.

Current Project/Future Work

This summer, I have been working with the LIMMBS Manipulation team's simulation of the self-righting work of Dr. Chad Kessens[1]. My goal is to add rough terrain to the simulation, and evaluate the resulting changes to the self-righting capability. The image in Figure 2 is an example of the terrain to be used. The blocks are a visualization of the surface within the PyBullet model.

[1] C. C. Kessens, D. C. Smith and P. R. Osteen, "A framework for autonomous self-righting of a generic robot on slipped planar surfaces," 2012 *IEEE International Conference on Robotics and Automation*, 2012, pp. 4724-4728, doi: 10.1109/ICRA.2012.6224778.

This terrain will be randomized between trials. This will be particularly useful for training the upcoming machine learning approach to the simulator's self-righting toolkit. Results were not yet available at the time of writing.

Acknowledgements

I'd like to thank Mr. Matt Kaplan and Dr. Chad Kessens for helping me through my numerous setbacks and technical difficulties this summer. Without them, I would not have been able to put this presentation together.

IMPROVING A SEMANTIC HIERARCHY ONTOLOGY BY RESOLVING HOMONYMS

POC: Seth Ellis, sellis7@umbc.edu
Mentor: Andre V. Harrison, andre.v.harrison2.civ@mail.mil

Motivation

- Autonomous vehicle systems can utilize the improved knowledge to increase efficiency in recognizing and prioritizing visual information
- Improving novel, zero-shot, few shot, and multi-class object recognition

Objectives

- Resolve homonyms to improve a semantic hierarchy ontology
- Reconstruct updated SUN hierarchy
- Train and Test hierarchical object recognition model using SUN hierarchy

Challenges

- Improving my Python acumen and knowledge
- How to resolve homonym labels without viewing every image
- Training on such a huge dataset required greater computational power

Approach

- Using Python, a visualization tool was created to identify if a label was a homonym
- Used Wordnet API to rebuild hierarchy
- Used an object recognition model to test hierarchal object recognition

Results

- Of the several hundred labels 17 homonyms were found, each of which defined 2-3 objects
- The full semantic hierarchy grew by 17 new nodes in total
- The simplified hierarchy grew by 14 new nodes

Homonym	Objects Found
Bed	Bed(Billiard Table), Bed(Truck Bed), & Bed(Sleeping)
Cap	Cap (Hat) & Cap(Plastic Cap)
Brush	Brush(Broom), Brush(Bush), Brush(Hairbrush), & Brush(Paintbrush)
Dish	Dish (Antenna) & Dish (Plate)
Face	Face(Clock face) & Face(Human)
Field	Field(Playing Field) & Field(Grass field)
Glass	Glass(Cup) & Glass(Windowpane)
Glasses	Glasses(Cups), Glasses(Sunglasses), & Glasses (Eyeglasses)
Keys	Keys(Lever) & Keys(Metal Instrument)
Pen	Pen(Writing Tool) & Pen (Enclosure)
Pitch	Pitch(Pitchers) & Pitch(Sports Field)
Runway	Runway(Fashion) & Runway(Airplane)
Shade	Shade(Shadow) & Shade(Lampshade)
Stall	Stall(Sale booth), Stall(Stable), & Stall(Witness Stand)
Stick	Stick(Gear-shifter) & Stick(Wood)
Suretcher	Stretcher(Framework) & Stretcher (Gurney)
Trunk	Trunk(Tree trunk) & Trunk(Chest)

Figure 1: Depicts the homonyms found and the objects the label defined in the dataset

Future Plans

- Train using randomized weights and biases
- Further train/test the subsequent custom pretrained model on other data
- Improve homonym recognition tool to automatically detect potential homonyms



Figure 2: Depicts the original hierarchy versus the new one (Green shows the new nodes added)

Conclusion/Discussion

- New nodes provided a brooder hierarchy to train the model
- New nodes also provide a more consistent pairing between label and example imagery
- The model is now exposed to more object labels and consequently knows more objects

Acknowledgements

- DoD/ARL
- Dr. Andre Harrison (Mentor)
- Eric Wilt & Darius Jefferson II

Measuring Thickness of III-Nitride Semiconductor Films for Lasers

Student: Lesly Henrriquez-Saravia, University of Maryland. College Park
Mentor: Dr. Gregory Garrett, SEDD

Objective

- To create smaller, compact and efficient semiconductor lasers to use for use in Quantum Information and Sensing system.
- To model the reflection properties of wide bandgap semiconductor films to determine their thickness. The films consist of c-AlN and c-GaN on top of a 3C-SiC substrate.

Method

- Found an equation that best modeled the reflectivity of dielectric layers in "Optics" by Paul Ewart.
- Consulted literature to find the index of refractions for each material.
- Equation for Reflection used is:

$$R = |r^2| = \left|\frac{An_0+Bn_0n_T-C-Dn_T}{An_0+Bn_0n_T+C+Dn_T}\right|^2,$$

with $k_1 = \frac{2\pi n_1}{\lambda}$, $A = \cos(k_1 t)$, $B = -i\left(\frac{1}{n_1}\right)\sin(k_1 t)$, $C = -in_1 \sin(k_1 t)$, and $D = \cos(k_1 t)$, where t = thickness. The refractive indices are n_0 = air, n_1 = index of the film, and n_T = index of the substrate

- Wrote a MATLAB script to model the reflection.
- Modeled the bottom layer consisting of 3C-SiC on top of a Si substrate first.
- Plotted the data and model in terms of energy to accurately measure the number of oscillations.
- Calculated four datasets with different thickness values, and found a linear relationship between thickness and the number of oscillations.
- Using this equation, We determined the thickness value for the 3C-SiC layer that produced a graph with the same number of oscillations in our collected data, as shown in Figure 1.
- Modeled the reflection for cubic-AlN, as shown in figure 2. We will use the same method to determine the thickness of the cubic-AlN and cubic-GaN films.

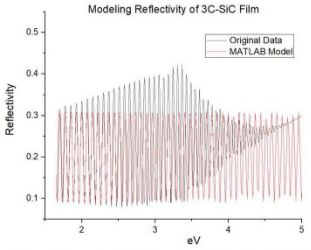


Figure 1: The graph in black shows the original data collected for the Reflectivity of the 3C-SiC layer. The graph in red shows the MATLAB model where thickness was set to 3284 nm.

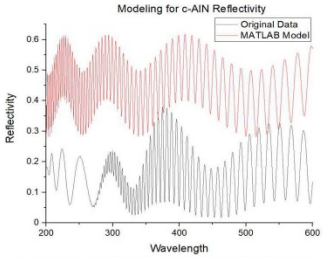


Figure 2: Original data for the reflectivity of the cubic-AlN layer is shown in black. The red graph is the MATLAB calculation with thickness set to 200 nm.

Results

- We determined the oscillations matched best when thickness equaled 3284 nm ± 162 nm for the 3C-SiC layer.
- As shown in Figure 2, we modeled the reflectivity of the c-AlN layer but need to refine the model to better match the data and calculate the thickness with better accuracy
- The absorption seen in the original data is not seen in the model. Modeling the absorption would get rid of the fast oscillation at shorter wavelengths making it easier to see the longer oscillation.

Conclusion

- Using this modeling technique, we can determine the thickness of semiconductor layers.
- We have determined the thickness of the 3C-SiC layer and plan to use the same method to determine the thickness for the c-AlN and c-GaN layers
- We plan to refine the model to provide a more accurate model for the two-layer system. We will consider other factors such as non-normal incidence and absorption.

Acknowledgments

I want to thank ARL for allowing me to participate in their research fellowship. I would also like to thank my mentor, Dr. Gregory Garrett, for guidance during this research.

References

1. Ewart, P. (2019). Chapter 10: Reflection at dielectric surfaces and boundaries. In Optics (pp. 10–1-10–4). essay, IOP Publishing Limited.
2. Hofmeister, A. M., Pitman, K. M., Goncharov, A. F., & Speck, A. K. (2009). Optical constants of silicon carbide for astrophysical applications. The Astrophysical Journal, 696(2), 1502–1516
3. Ababneh, A., Albataineh, Z., Dagamseh, A. M. K., Al-kofahi, I. S., Schäfer, B., Zengerle, T., Bauer, K., & Seidel, H. (2020). Optical characterization of sputtered aluminum nitride thin films – correlating refractive index with degree of c-axis orientation. Thin Solid Films, 693, 137701.

Meta-Learning: Combining MAML and Langevin Dynamics

Student Intern: Christine Kwon
Mentor: Dr. Jemin George

Motivation

An adequate machine learning model is trained on copious amounts of data. However, the learning rate of humans is significantly faster and requires only a few examples to learn from. Meta-learning aims to emulate this, learning from only a few training examples. However, this process is bound result in uncertainty due to training on such few samples. We aim to build an algorithm that captures both the quick learning and adaptation to new tasks and uncertainty that may result from learning from a few training samples.

Langevin Dynamics

Langevin Dynamics is a class of Markov chain Monte Carlo (MCMC) techniques, which takes the Bayesian approach to capture parameter uncertainty. This approach updates the model's parameters through steps of gradient descent, similar to the MAML algorithm, but it incorporates Gaussian noise in its algorithm to account for parameter uncertainty.

$$\Delta\theta_t = \frac{\epsilon_t}{2}\left(\nabla \log p(\theta_t) + \frac{N}{n}\sum_{i=1}^{n} \nabla \log p(x_{ti}|\theta_t)\right) + \eta_t$$
$$\eta_t \sim N(0, \epsilon_t) \qquad (4)$$

Background

Meta-learning imitates the human learning process, its ability to learn concepts and attain knowledge from only a few examples. In other words, meta-learning allows quick learning from small amounts of data and prior experience, further accommodating to newly available data.





Method

The advantage of the MAML algorithm is its ability to quickly adapt to new tasks, to achieve fast learning. However, it does not account for the parameter uncertainty that may arise. To solve this issue, we additionally introduce Langevin Dynamics to capture parameter uncertainty. The combination of both these algorithms allows for quick adaptation to a new task and inclusion of parameter uncertainty given few training examples.

Model Agnostic Meta-Learning (MAML)

The MAML algorithm is a significant and commonly used meta-learning algorithm, which trains a model to rapidly learn from a few-shot learning problem. This algorithm trains the model's initial parameters through gradient descent to achieve fast learning on a new task.



Future Visions

We envision an algorithm that incorporates both MAML and Langevin dynamics and incorporate to different types of datasets to observe its overall performance. We look to further find more accurate methods to enhance meta-learning algorithms.



Acknowledgements

I would like to thank…
- My mentor, Dr. Jemin George
- Army Reserach Laboratory

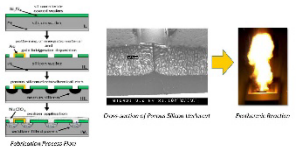
UNCLASSIFIED

Automation of Measurement Tools for Porous Silicon Characterization

Ms. Janelle Mabrey, Hampton University
Mentor: Dr. Wayne Churaman, DEVCOM ARL-ALC

Background

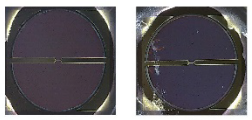
- Nanostructured porous silicon is a high surface area material that is normally insert, and becomes energetic when infused with an oxidizer such as sodium perchlorate.
- The pores are formed using a electrochemical etch process that involves submerging a patterned silicon nitride wafers in a bath containing hydrofluoric acid, ethanol, and peroxide.
- A micropipette is used to drop-cast the oxidizer into the nano-pores, which range in diameter from 3-4 nm.
- A bridgewire integrated along the porous silicon is induced with a current that fractures the pores, causing the silicon fuel and oxidizer to mix.
- The resulting exothermic reaction generates a controlled shockwave that can be harnessed for application such as fuzing.



Fabrication Process Flow | *Cross-sectional Porous Silicon Structure* | *Bridgewire Reaction*

Motivation/Objective

- The Pyro Electronics Team is developing porous silicon initiators.
- ARL and collaborators have undertaken pilot production to manufacture and evaluate over 1,000 initiators.

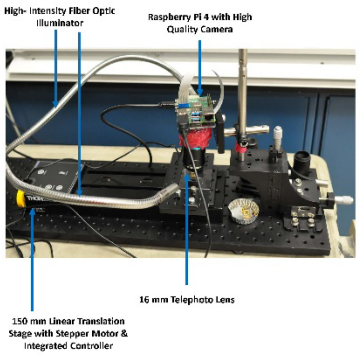


Unetched PSi | *Etched PSi*

- The program aims to develop a semi-automated system to provide image acquisition for quality assurance in a stable dry box environment because of the moisture sensitivity of the oxidizer.
- Images will later be used to develop machine learning algorithms that recognize porous silicon and bridgewire failures.

Experimental System

Semi-Automated Device Inspection System



Capture Tool

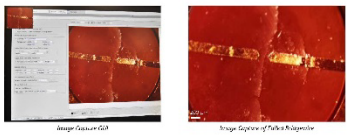


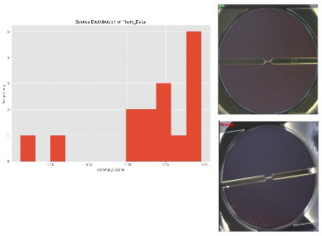
Image Capture GUI | *Image Capture of Failed Bridgewire*

- Image capture of the device displays delamination of bridgewire in the center region and surface cracking along the porous silicon.

Anomaly Detection

Isolation Forest – Outlier Detection

- The Anomaly Detection routine uses the Isolation Forest algorithm to detect anomalies. Partitions are recursively generated on datasets in order to isolate outliers whose smaller paths set them apart from normal data.
- The anomaly score can help to set a threshold for a routine to determine outliers negative numbers are more likely to be outliers while positive ones are more likely to be normal.
- A larger dataset is needed to train the model and conduct testing.



Pathway Forward

- Collect more images of both successful and failed devices along with their bridgewires to increase dataset for machine learning algorithm.
- Further develop and improve efficiency of Anomaly Detection routine.
- Further develop Device Inspection System to include enclosed dry box, longer translation stage, better camera attachment, and humidity/temperature sensor

Acknowledgements

I would like to acknowledge my CCDC ARL Mentor, Dr. Wayne Churaman for his guidance and assistance during this summer internship. I would also like to acknowledge the CCDC-ARL as well as the DOD HBCU/MI Summer Research Program for providing this research opportunity.

UNCLASSIFIED

Design of MAX Reinforced High-Performance Steel Composites for Sliding Applications

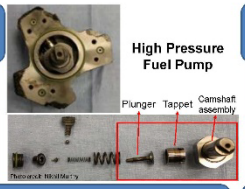
Caleb Matzke
Mechanical Engineering
University of North Dakota

UND Advisor: Dr. Surojit Gupta
Assoc. Prof. of Mechanical Engineering
University of North Dakota

ARL Mentor: Dr. Stephen Berkebile
Directorate / Division: CISD/ VICTOR ERP
Project Duration: 06/01/2021 to 08/20/2020

Motivation

- High pressure fuel pumps are a vital component in Unmanned Aerial Systems
- Wear and scuffing are major issues due to low lubricity fuel in fuel pumps, fuel injectors and valves [1]
- Lubricity = Chemistry + Viscosity + Solid Lubricants
- Chemistry varies between fuels which results in different material interactions (polar, non-polar, etc.)
- Viscosity directly affects friction and fluid film thickness



Objective

- **Overall:** Expand operational capabilities to increase lifetime and robustness of diesel fuel systems run with lower viscosity fuel
- **Objective:** Determine the microstructure and its effect on wear and coefficient of friction of 52100 steel - MAX phase composites (52100 steel – 5 vol% Cr_2AlC) lubricated by fuels of different chemistries (alkane, alcohol, hydrocarbon mix)
- **Hypothesis:** Addition of MAX phase additions will increase the hardness and Tribological properties of 52100 steel composites

Background

MAX phases
- Ternary solids
- Used to enhance tribological properties
- Desirable properties
  - Highly Damage resistant
  - Creep resistant
  - Readily machinable
  - Conductive
  - High oxidation resistance
- MAX phases of interest
  - Cr_2AlC (MAX phase)
  - These show promising wear results during dry sliding
- The MAX/MAB phases are being used as reinforcements in composites

52100 STEEL MAX-PHASE COMPOSITES
- Novel 52100 Steel - MAX phase composites
- Heat treatment is done to improve hardness
- liquid lubrication studies are conducted using Ethanol, F-24, and Dodecane

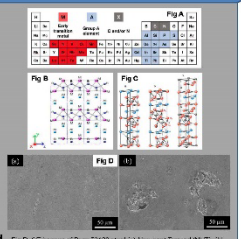
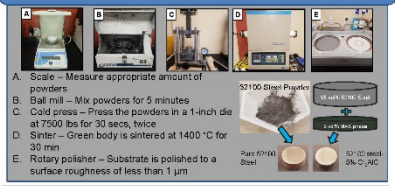


Fig D. SEI images of Pure 52100 steel (a) Non-heat Treated (NHT) (b) Heat Treated (HT)

Samples prepared by Emily Dahlke at Abdurahman Aldossary

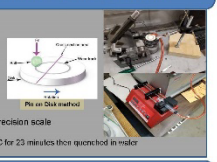
Manufacturing Process



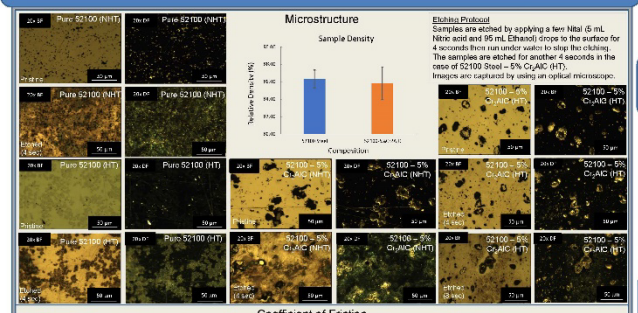
A. Scale – Measure appropriate amount of powders
B. Ball mill – Mix powders for 5 minutes
C. Cold press – Press the powders in a 1-inch die at 7500 lbs for 30 secs, twice
D. Sinter – Green body is sintered at 1400 °C for 30 min
E. Rotary polisher – Substrate is polished to a surface roughness of less than 1 µm

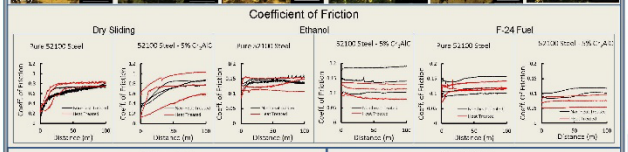
Experimental Method

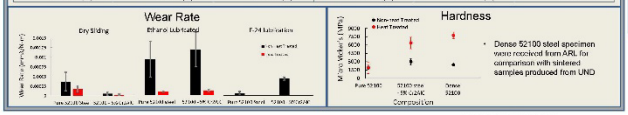
- CSM Instruments Tribometer
  - Linear velocity: 20 cm/s
  - Sliding distance of 100 m
  - Load of 5 N
  - Disk radius of 4 mm
  - 6 mm diameter alumina ball
- Syringe Pump
  - Lubricant flow rate of 0.5 mL/min
  - Dry, Ethanol, F-24 fuel
- Wear
  - Measure weight before and after with precision scale
- Heat Treatment
  - box furnace used to heat specimen to 840 °C for 23 minutes then quenched in water



Results







Discussion and Conclusions

- Samples are not fully dense, resulting in micropores
- Etching reveals micron size grains in the both heat treated and non-heat treated steel compositions
- The addition of 5 vol% Cr_2AlC increases the overall hardness in the case of both heat treated and non-heat treated samples
- 52100 steel - 5 vol% Cr_2AlC have comparable hardness to heat treated dense 52100 steel
- Ethanol lubrication has poor tribological compatibility with 52100 steel since it displays an increase in wear compared to dry sliding in non-heat treated specimen. However, heat treated specimen showed similar wear as compared to dry sliding
- Non-heat treated specimen run under F-24 lubrication show comparable wear results as to dry sliding. Wear of heat treated specimen under F-24 lubrication could not be determined by using our current method

Path Forward

- Produce high density specimen through other processes such as hot isostatic pressing
- Perform Atomic force microscopy on F-24 lubricated specimen to determine wear caused by the tribological experiments
- Complete dodecane lubricated tribological experiments
- Perform SEM analysis on etched specimen
- Perform high intensity tribological experiments by increasing the sliding distance and applied load

Acknowledgements

Other contributors
Nikhil Murthy, Emily Dahlke, Abdurahman Aldossary Maharshi Dey
Funding Sources
Dean Professorship awarded to Dr. Gupta.
Army Educational Outreach Program College Qualified Leaders and Oak Ridge Associated Universities

[1] Qi, J. et al. (2005). Wear, 258(7–8), 1084–1092.

Back-Face Deformation Analysis

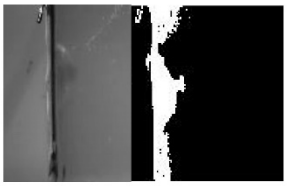
Adam Menkara, Biomedical Engineering
Mentor: Dr. Karin Rafaels
WMRD – Soldier Protection Sciences Branch

Motivation

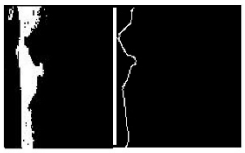
- Behind armor blunt trauma (BABT) can occur behind soft or hard ballistic vests and can result in severe injuries
- Current analysis techniques of back-face deformation involving ballistic gelatin video has a limited signal to noise ratio and require lots of time to process
- Modern programs that perform this analysis are hard to use and require lots of processing power because of the limited data found within individual frames at very high rate of capture (fps)

Methodology

- Programming in Python allows for the use of a vast range of libraries and tools not available to other languages such as MATLAB
- Rather than looking at individual frames within the video and applying many post-processing filters, we can find the difference between 2 frames of the video to detect movement

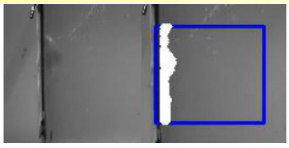


- Applying a gaussian blur filter aids in removing noise at the edge of the deformation
- Then, we can analyze each individual pixel by creating a 3x3 matrix around each, and measuring for brightness changes across adjacent pixels to create an edge



- Finally, we can define a region of interest to limit the computational power required and reduce noise.
- We can measure the number of pixels until an edge is detected along each horizontal row in the region of interest and log those numbers for analysis

Results



- Comparing the original video and the computer interpretation of the edge, there is little under/overlapping of the image and shows the accuracy of the tracking algorithm
- The current most reliable method to track the edge is by hand, which can take upwards of 5 hours in total to analyze one video. This method was able to generate data on high fps BABT videos in under 5 minutes.
- A sample of 6 BABT videos were analyzed using the new program and was successful in tracking 5 deformations accurately.

Conclusion

- The tracking algorithm is able to quickly and successfully track edges across a range of different video qualities and provide data for further analysis
- This video analysis method can be used for applications other than this such as analysis of flash x-rays

Acknowledgment

- I would like to thank ARL for the opportunity to participate in meaningful research that will hopefully benefit our armed forces.
- A special thank you to Dr. Karin Rafaels, Dr. Cynthia Bir and Dr. Alan Goertz for their guidance and support throughout this project.

UNCLASSIFIED

Terrain Aware Costmap Generation for Unmanned Ground Vehicles using Multimodal Inverse Reinforcement Learning

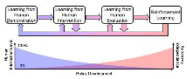
Ashwin Menon, University of Rochester
Maggie Wigness, PhD, ARL



Robust human-robot teams allow soldiers to focus on higher-level tasks

Objectives

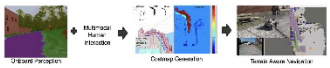
- We want to increase the level of autonomy for UGVs in order to create a more dependable and robust soldier teammate. Thus we try to answer the following questions
  - Can global planning trajectories which use multimodal inverse reinforcement learning (mIRL) improve optimality when compared to demonstration-only or intervention-only approaches?
  - Can an algorithm be designed which efficiently uses both human demonstration and intervention based on incoming perceptual data?
  - Does the mIRL approach make the offline training process faster due to less perceptual and odom data than learning from demonstration (LfD)?



Above: [3] The Cycle of Learning paradigm. mIRL makes use of only LfD and LfI

Related Works

The Goecks publication [3] is novel in that it makes use of the multimodal approach. APPLD[1] and APPLI[2] use only demonstration and intervention, respectively, in the context of learning local control parameters. The results shown in Wigness[4] are what we hope to optimize on with the mIRL methodology. While Goecks' approach is similar to ours, it is used in a completely different application space and makes use of a different type of learning process. It attempts to optimize on an autonomous perching task for unmanned aerial vehicles (UAVs) and uses behavior cloning (BC). BC has the robot attempt to mimic the demonstrator across the entire state space. IRL, however, attempts to infer the goal state based on the demonstrator. Conversely, our approach is aimed at optimizing costmap generation for UGVs and we make use of the IRL paradigm.

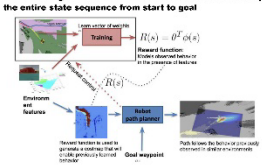


Above: [4] High-level overview of mIRL

Approach

- Leverage multimodal inverse reinforcement learning (mIRL) to robustly learn behavior reward functions based on:
  - incoming perceptual data
  - optimal policy exemplified by human demonstrations and interventions
- Reward function learning for taking a given path is the the sum of the rewards at each state (it's linear): $R(\zeta) = \sum_{s_t \in \zeta} R(s_t)$
- Intuition: reinforcement learning is the task of behaving optimally based on a given reward function. IRL is the opposite task of extracting a reward function based on demonstrated optimal behavior

Below: [4] A flowchart of the online intervention paradigm. Note that the human expert can dynamically update the reward function online in this framework. The demonstration paradigm can be thought of as the offline version of this while spanning the entire state sequence from start to goal



Demonstrations and Interventions

- Demonstration
  - Human expert proactively teleoperating robot in order to provide optimal planning policy
  - PRO: Offers a very richly defined trajectory to robot
  - CON: Requires more data to achieve mission success
- Intervention
  - Human expert reactively teleoperating in order to provide corrective actions to robot moving autonomously
  - CON: Robot isn't offered optimal policy to the same level of detail as demo
  - PRO: Requires less data to achieve mission success

Experimental Setup

- Wheeled mobile robot teamed with human expert (following optimal policy) tasked with finding optimal global plan to goal state via an inverse reinforcement learning paradigm
- Robot will be tested in a Unity-powered simulator that represents a real-world environment
- Optimal plan is a weighted metric of path length, terrain type (eg. grass, gravel, and asphalt), and terrain elevation
- Two human datasets are accumulated - demo dataset and intervention dataset
  - When expert decides a certain chunk of a trajectory requires intervention, a joystick button is pressed to switch robot data collection into intervention dataset (default human dataset is demo)



Left: an example of the Warthog UGV in the Unity simulator. Terrain type is grass.

Experimental Metrics

- Modified Hausdorff distances - path similarity - (MHD) are measured and then compared against teleoperated ground truth trajectories (B is GT trajectory, A is trajectory to be compared

$$h(A,B) = \frac{1}{|A|} \sum_{a_i \in A} \{ \min_{b_j \in B} d(a_i, b_j) \},$$

  - Learning from demonstration vs. ground truth
  - Learning from intervention vs. ground truth
  - mIRL vs. ground truth
- Training times are recorded to determine whether the mIRL approach trains offline faster than the LfD approach

Hypothesis

- We expect to see the following outcomes
  - A significant decrease in MHD when comparing mIRL-planned trajectories vs. intervention-planned trajectories
  - A negligible difference in MHD when comparing mIRL-planned trajectories vs. demo-planned trajectories
  - A significant decrease in training data required for successful waypoint navigation when comparing the mIRL paradigm to the LfD paradigm
  - A negligible difference in training data required for successful waypoint navigation when comparing the mIRL paradigm to the LfI paradigm

References
- [1] Xiao, Xuesu, et al. "Appli: Adaptive planner parameter learning from demonstration." *IEEE Robotics and Automation Letters* 5.3 (2020): 4541-4547.
- [2]Wong, Fisher, et al. "Appli: Adaptive planner parameter learning from interventions." *arXiv preprint arXiv:2011.03499* (2020).
- [3]Goecks, Vinicius G., et al. "Efficiently combining human demonstrations and interventions for safe training of autonomous systems in real-time." *Proceedings of the AAAI Conference on Artificial Intelligence*. Vol. 33. No. 01. 2019.
- [4] Wigness, Maggie, John G. Rogers, and Luis E. Navarro-Serment. "Robot navigation from human demonstration: Learning control behaviors." *2018 IEEE International Conference on Robotics and Automation (ICRA)*. IEEE, 2018.

UNCLASSIFIED

Approved for public release: distribution unlimited

Effect of Sample Morphology on the Plasma Hydrodynamics of Al_2O_3

Clayton Miller,[1] Elliot Wainwright,[2] Jennifer Gottfried[2]

[1]Texas Tech University
[2]DEVCOM ARL, FCDD-RLW-WA

INTRODUCTION

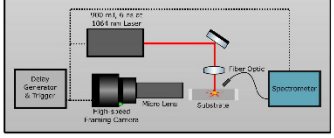
The differing behavior in hydrodynamics of the plasma resulting from the laser-induced air shock of micro- and nano-sized particles of non-reactive alumina (Al_2O_3) is explored. Previously, the laser-induced plasma plume of different sized reactive aluminum particles was imaged and shown to have certain species in different regions of the plume (Wainwright et al, 2020). In this study, we explore the effect of particle size vs. chemistry on the hydrodynamics of the plasma by comparing the plasma of Al_2O_3 to that of the previously observed aluminum.

Wainwright, E.R. et al. Effect of sample morphology on the spectral and species-specific characteristics of laser-induced plasmas from aluminum. Appl. Phys. A 126, 83 (2020).

METHODOLOGY

Laser-induced air shock from energetic materials (LASEM)

- Sample: Several milligrams of powder pressed onto double sided tape which is affixed to a glass slide.
- A high energy laser pulse (Quantel Brilliant B, 1064nm, 6ns pulsewidth, ~660mJ, ~60J/cm^2 fluence) is used to ablate the sample.
- Plasma hydrodynamics were imaged using a high speed framing camera (PCO, HSFC Pro).



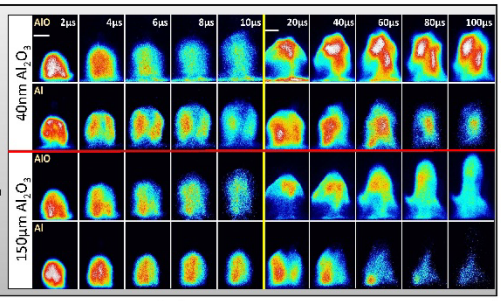
PLASMA IMAGING

Plasma is imaged using band pass filters at wavelengths at which species of interest are known to emit.

- AlO – 480nm
- Al – 400nm

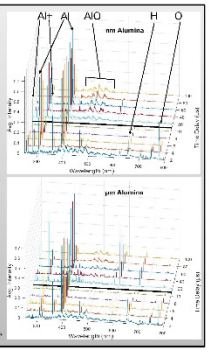
Most notable is the difference between the AlO emission regions for nano vs micro-alumina. (Camera exposure increased at yellow line.)

Scale bar for each time regime is 500µm.



GATED SPECTROSCOPY

Spectra are recorded at increasing time steps for each sample. The max intensities of the spectra are off scale to highlight the lower intensity emission. The solid black line indicates the gate width increase at the later timescale of the spectrometer in use.



CONCLUSIONS

- Particle size has a clear impact on the hydrodynamics of the plasma resulting from the laser ablation of a specific material.
- Some mechanism is keeping a portion of the AlO emission close to the sample slide for only the ablated nano-alumina.
- The nano-alumina has distinct intense regions of emission for both species mapped. This stronger intensity is also reflected in the spatially integrated spectra emitted by the smaller particle size.
- The AlO forms where the Al is weaker, showing that the Al is cooling to form AlO.
- Plasma plume growth of the micro-alumina is driven by a strong vortex ring based on the shape of the late stage plasma plume.

Approved for Public Release: Distribution Unlimited

Effect of Aluminum + Graphene Oxide Reactive Material Sample Preparation on Electrostatic Sensitivity

By Kristi Naude, Dr. Elliot Wainwright, and Dr. Jennifer Gottfried

Motivation

- The development of next generation munitions [Ref 1] requires developing and testing novel reactive materials to ensure safe operation
- Current methods of using tape cracks to quantify novel reactive material electrostatic sensitivity is inherently subjective in nature
- An objective method of confirming samples' detonation (go) or non-detonation (no-go) status is required to ensure operator safety

Experimental Setup

- Electro-Tech Systems Model 931 Firing System (4mJ-10.5J range tested)
- Two photodiodes (486nm and IR)
- Two high-speed cameras (10kFPS, 1µs shutter)

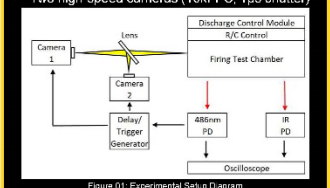


Figure 01: Experimental Setup Diagram

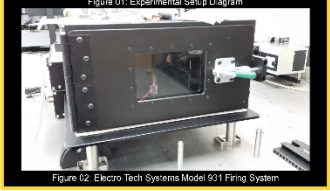


Figure 02: Electro-Tech Systems Model 931 Firing System

Results

Al+GO Sample: Physically Mixed



Figure 03: Al-GO Physically Mixed Sample Ignition

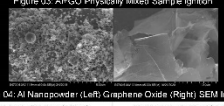


Figure 04: Al Nanopowder (Left) Graphene Oxide (Right) SEM Images

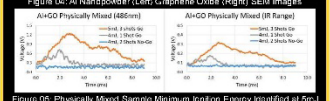


Figure 05: Physically Mixed Sample Minimum Ignition Energy Identified at 5mJ

Al+GO Sample: Graphene Oxide Coated

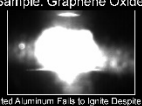


Figure 06: GO-Coated Aluminum Fails to Ignite Despite Massive Discharge

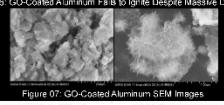


Figure 07: GO-Costed Aluminum SEM Images

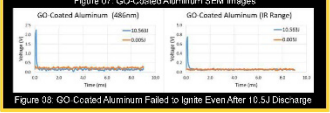


Figure 08: GO Coated Aluminum Failed to Ignite Even After 10.5J Discharge

Objective Criteria

- Used photodiode traces to confirm go or no-go test results
- Initial spike caused by the electrostatic discharge, with initial signal intensity proportional to discharge energy
- The presence of a time-delayed signal occurring after ~0.3ms, when the discharge signal had dissipated, confirmed the test was a "go"
- Lack of any signal after ~0.3ms confirmed the test was a "no-go"

Conclusions

- The physically mixed Al+GO sample exhibited significantly greater electrostatic sensitivity, igniting once in three shots at 4mJ discharge and all three shots at 5mJ discharge
- The GO-Coated Aluminum didn't ignite at any point during testing, even when exposed to a 10.5J discharge
- According to previous work conducted by Eric S. Collins et al., [ref 2], the graphene nanoplatelets covering the 3.0-4.5 micron aluminum acts as a redirector for the electrical discharge, thereby preventing the internal reactive aluminum from being ignited
- It is hypothesized that the same mechanism is affecting the electrostatic sensitivity of the current samples of 110nm aluminum wrapped in graphene oxide

References

1. Jiang, Yue, et al. "Energetic Performance of Optically Activated Aluminum/Graphene Oxide Composites." *ACS Nano*, vol. 12, no. 11, 2018, pp. 11366–11375., doi:10.1021/acsnano.8b06217.
2. Collins, E. S., Skelton, B. R., Pantoya, M. L., Irin, F., Green, M. J., & Daniels, M. A. (2015). Ignition Sensitivity and Electrical Conductivity of an Aluminum Fluoropolymer Reactive Material With Carbon Nanofibers. *Combustion and Flame*, *162*(4), 1417–1421., doi:10.1021/acsnano.8b06217
3. Lily Giri credited for acquiring the SEM images

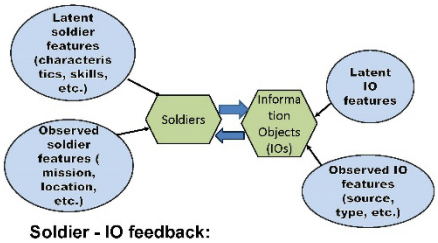
Approved for Public Release: Distribution Unlimited

RESEARCH ON DETERMINING ADAPTIVE VALUE OF INFORMATION

ARL Mentor: Jade Freeman jade.l.freeman2.civ@mail.mil
Summer Intern: Konstantinos Pantazis kpantazi@umd.edu
Directorate: CISD

Research Objective

- Towards addressing the problem on information overload in tactical environment, this research seeks to find an algorithmic approach to quickly target critical operational information for dissemination over C3I networks.
- The **main objective** is to considering Value of Information (VoI) problem as a **recommendation task problem** and hence, incorporate state-of-the-art methods from the Recommender Systems' literature.



Soldier - IO feedback:

$$\text{Reward} = f(Soldier, IO) + \text{Noise}$$
where f similarity function.

Motivation

- Recent advancements in Data collection techniques have resulted to low-cost, large-scale and heterogeneous datasets to which tactical networks are unable to process in a timely manner.
- The notion of the ***value of information*** (VoI) is developed to support effective communications in tactical networks.
- VoI-based methods focus on the challenging problem of prioritizing and filtering valuable information to and from dis-mounted soldiers in a battlefield environment.

Background

- *Policy-based* VoI approaches have been developed to combat information overload and to reduce bandwidth based on *a priori* mission contexts using deterministic approach.
- Recently, automated procedures such as *Contextual Multi-Armed Bandits* (CMAB) have been proposed to complement existing approaches. Yet, they do not take into account
  - soldier relational data,
  - arrival of new soldiers and
  - time-evolving environments.

Proposed methodology

1. Develop a graph representation which encodes the mutual relations among soldiers [1] and implement **collaborative filtering** via matrix factorization techniques to account for the relations among soldiers into the reward function.

$$\text{Reward} = f(Soldier's\ peers, IO) + f(Soldier, IO) + \text{Noise}$$

2. Incorporation of a *drift term w* [3] to simulate changes in soldier's preferences over time.

$$\text{Reward} = w\left[f(Soldier's\ peers, IO) + f(Soldier, IO)\right] + \text{Noise}$$

3. Integration of Combinatorial CMAB schemes such as CUCB [2] for multiple-object recommendation.

Future work

- Appropriately integrate the proposed methodology into a *learning algorithm (Combinatorial CMAB)* for prioritizing and filtering IO in dynamic tactical networking environments.
- Provide desirable theoretical guarantees such as *optimal regret bounds*.
- Evaluate algorithm's performance empirically and/or theoretically based on simulations.

Acknowledgements

- I thank Dr. Jade Freeman for her guidance and help throughout summer.
- I also thank ARL's internship program for providing students the opportunity to participate in meaningful and hands-on research.

References

[1] H. Wang, Q. Wu, H. Wang. *Factorization Bandits for Interactive Recommendation.* AAAI 2017

[2] W. Chen, Y. Wang, Y. Yuan. *Combinatorial Multi-Armed Bandit: General Framework. Results and Applications.* PMLR 2013

[3] Q. Wang, C. Zeng, W. Zhou, T. Li, L. Shwartz, G. Y. Grabarnik. *Online Context-Aware Recommendation with Time Varying Multi-Armed Bandits.* KDD'16

Scene Understanding for Threat Classification for Natural Disaster Images

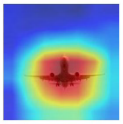
Abhay Patel, University of Maryland College Park – DoD Researcher, apatel49@terpmail.umd.edu
Mentor: Dr. Adrienne Raglin, US Army DEVCOM Army Research Laboratory, Artificial Reasoning Team Lead

Motivation/Objective

- Computer vision techniques handle tasks such as classification and detection.
- Scene understanding of images through computer vision is particularly complex.



Un-Labeled Image



Labeled Image

The research objective is to create a model that uses causal reasoning for scene understanding to classify threats.

Rationale

- Current scene understanding techniques can detect and classify multiple objects and their context within an image.
- We can create datasets that emulate natural threats by using images of natural settings that may contain indications of natural disasters.
- ***Our approach is to layer an object classification model within a deep neural network (DNN) that uses causal reasoning to identify threats.***

Results

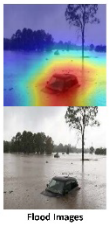
- Visual indicators of threat-related object in natural disaster are not always detected.
- Best performance for fire related images with accuracy of roughly 90% across samples.
- Roughly 20% accuracy across samples indicates challenges for flood and earthquake images (i.e. problems detecting water) as well as earthquake images.
- Lowest classification for image of floods and earthquakes due to subtle cues.



Example Labeled Fire Image

Discussion/Conclusion

- Implementing a dense model allows classification of each pixel, allowing for the water in the flood images and rubble in earthquake images to be detected.
- Utilizing a model that learns intended subtle visual cues may improve performance for specifically flood and earthquake related images.
- Retraining an existing causal reasoning based model may improve performance for learning visual cues that indicate threats for these types of scenes.



Flood Images

Pathway Forward

- Define robust models to ensure transferability of the model to different classes of images.
- Analyze the results from the causal reasoning approach to see what cues the model learns.
- Evaluate the multiple object classification to ensure key objects are detected.
- Explore data augmentation techniques that preserve visual cues to address data limitation while ensuring the desired causal relationship is learned.
- Utilize causal exploration to improve performance of scene understanding to identify threat scenes.

Acknowledgements

- J. Long, E. Shelhamer, and T. Darrell. Fully convolutional networks for semantic segmentation. In CVPR, 2015.
- L. Li, R. Socher and L. Fei-Fei, "Towards total scene understanding: Classification, annotation and segmentation in an automatic framework," 2009 IEEE Conference on Computer Vision and Pattern Recognition, 2009, pp. 2036-2043.
- R. Vedantam, K. Desai, S. Lee, M. Rohrbach, D. Batra, and D. Parikh, "Probabilistic neural-symbolic models for interpretable visual question answering," in Proc. ICML, 2018.

Fabrication, Testing, and Application of Betavoltaic Devices

Student: Jeffrey Read Mentor: Marc Litz

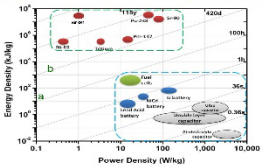
Abstract

Betavoltaics are a power source that harnesses energy from radioisotopes to produce electric power. Since radioisotopes emit high-energy particles for long periods of time, these devices are ideal for extended duration sensing or medical implants. While semiconductor materials are readily available to harness the particles, consistent fabrication and packaging of prototypes is still a challenge and will require new manufacturing techniques for higher density integration. Of the available semiconductor materials, InGaP is best suited to our needs and is cheap and available. The I-V curves were generated for 1 cm2 semiconductor chips to determine diode quality and response characteristics. To contain the radioisotope on top of the semiconductor, we fabricated reservoirs from UV cured resin in specially designed Silicone molds. The mold required design of a 3D printed fixture. Reservoirs were sealed to the InGaP devices that were then mounted on copper groundplanes. Wire bonding from InGaP to groundplane completed the electrical connection in the device fabrication process. With the device fully fabricated, we can add radioisotope to complete the betavoltaic. Future efforts will investigate stacking and their connections along with arrays towards the goal of 10mW/cc power sources to operate devices for long-term military applications.

Overview

- Betas transfer kinetic energy to the semiconductor, freeing electrons. The electrons hole pairs (EHP) near the depletion region then separate due to the built-in p-n junction and flow to the negative and positive sides, respectively.
- Semiconductor options include InGaP, SiC, GaN, ZnO, and more, which all vary in bandgap
- The semiconductor must have a depletion region for current to be induced

Tritium is an ideal power source because it has the lowest energy betas and is the least biotoxic



Testing

Each InGaP must be tested to determine whether the device responds as a diode, resistor or open circuit. On an IV-chart:

- The resistors start at a high current, drop to zero current at zero volts, then continue the linear current drop with voltage.
- A diode will begin with a low current then suddenly switch on somewhere between 0.7 and 0.8 volts and conduct electricity much more freely
- An open circuit will conduct minimal current and never switch on



FIG 4 The Raspberry Pi, Keithly 2450 sourcemeter, and splitter device are shown in the picture on the far left, attached to a display where user work with the RPi and deal with the program

FIG 5 The testing probe, back contact, and (broken) wafer are shown as well

We must determine if each semiconductor is a low-leakage diode

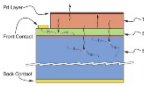


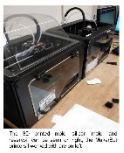
FIG 3 Schematic of Betavoltaic device structure. The tritium layer sits adjacent to the p-n junction, which is shown in red. The front contact collects the holes and the back contact collects the electrons.

Summary

- Betavoltaics are power sources that enable sensors to operate in remote locations for many years without maintenance
- Beta emitting radioisotopes are the easiest decay product to shield and are safe for soldier operations
- Increasing the energy density of these power sources is dependent on our ability to manufacture arrays or stacks of these devices
- We've explored several techniques to fabricate these arrays for the highest energy density power source
- Packaging these devices is a tricky yet necessary final step towards applying Betavoltaics to military applications

Reservoirs

- In order to contain the liquid Ni-63 or Tritium, we need to make and secure a UV cure epoxy reservoir to the InGaP
- UV cured epoxy is a strong but soft material perfect for use on delicate semiconductors



- First, I 3D printed a mold which we could then fill with silicon
- Once this solidified, we had a silicon mold which we could fill with epoxy to make reservoirs
- The epoxy doesn't stick to silicon, which is why it was necessary to use a silicon mold

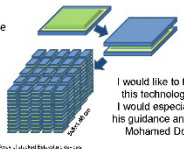


3D printing was a necessary skill to learn for device manufacturing

PV Device Mounting

- The manufacturing process includes carving a copper coupon to separate the positive and negative
- Silver epoxy is used to attach the device to the copper board
- Positive side is then wedge bonded to contact bar on device
- Wires are sauntered to the copper board
- Final step includes epoxying previously shown reservoirs to center of device using UV cure epoxy





Acknowledgements

I would like to thank ARL for allowing me to learn about this technology and providing the resources to do so. I would especially like to thank my mentor Marc Litz for his guidance and expertise, as well as Randy Thompson, Mohamed Doumbia, and Muhammad Khan for their immeasurable help

[1] Christopher I. Thomas, Samuel Portnoff, and M. G. Spencer, "High efficiency 4H-SiC betavoltaic power sources using tritium radioisotopes," Applied Physics Letters 108, 013505, 2016.

NMR Structural Determination of a Cyclometalated Iridium(III) Complex

Student: William R. Roberts, wrrobert@buffalo.edu
Mentors: Dr. Ryan M. O'Donnell, ryan.m.odonnell12.civ@mail.mil
Dr. Thomas Rohrabaugh, Jr., thomas.n.rohrabaugh.civ@mail.mil

Background

Common applications for cyclometalated iridium(III) complexes include solar cells/solar energy conversion, photodynamic therapy, and electrophosphorescence. The last of these is particularly important, as it represents these complexes' use in organic light emitting diodes (OLEDs).[1]

These complexes are of interest for Army applications due to their non-linear optical properties. Those allow for their uses as reverse-saturable absorbers (RSAs) and two-photon absorbers. RSAs undergo photophysical changes upon absorption of a photon, transforming it into a slightly modified form of the species which is capable of absorbing light with increased efficiency.

Because traditional benchtop methods for synthesizing these complexes commonly involve reaction times of hours or even days, increasing the synthetic efficiency of these complexes is of great interest.

NMR Spectroscopy

NMR (Nuclear Magnetic Resonance) spectroscopy encompasses a variety of experiments, all of which focus on analyzing the electronic environment of all nuclei of a given type in a sample. The instrument (an example of which is shown below) uses a combination of magnetic fields and radio wave detectors to generate a spectrum. This spectrum is unique for each species, making it a common method for determining whether a given product has been generated, and what, if any, impurities might also be present.

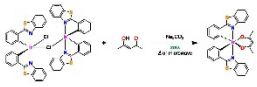
Commonly, multiple experiments will be used in tandem, as each gives different insight into the structure.



References

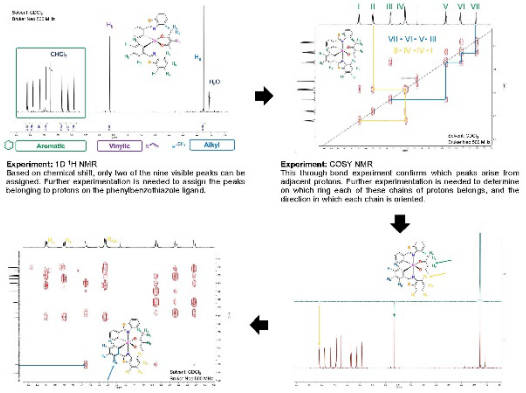
1. Reddy, M. L. P.; Sebyomohandas, K. S., Evolution of 2, 3′ bipyridine class of cyclometalating ligands as efficient phosphorescent iridium(III) emitters for applications in organic light emitting diodes. *Journal of Photochemistry and Photobiology C: Photochemistry Reviews* **2016**, *29*, 29-47.
2. Bruker.com NMR in Forensic Analysis. https://www.bruker.com/ru/resources/library/application-notes-nmr/nmr-in-forensic-analysis.html (accessed 22 Jul 2021).

Inspiration



The focus of the original investigation was the effects of manipulating solvent properties (particularly boiling point) on the microwave-assisted synthesis shown at left. The goal of this investigation was to find a microwave solvent which yielded the optimal tradeoff of product yield and purity, solvent cost, and environmental impact. In the process of analyzing the samples produced using each of these solvents, it was discovered that complete NMR analysis had not yet been reported for the intended product, [Ir(ppy)$_2$(acac)]. In order to be better able to analyze these samples, all relevant peaks in the ^{1}H NMR spectrum of this species were definitively assigned using the characterization routine shown below.

Characterization Routine



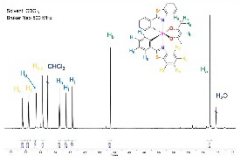
Experiment: 1D ^{1}H NMR
Based on chemical shift, only two of the nine visible peaks can be assigned. Further experimentation is needed to assign the peaks belonging to protons on the phenylbenzothiazole ligand.

Experiment: COSY NMR
This through bond experiment confirms which peaks arise from adjacent protons. Further experimentation is needed to determine on which ring each of these chains of protons belongs, and the direction in which each chain is oriented.

Experiment: ^{13}C – HMBC NMR
This first through bond experiment allows for definitive assignment of the peaks arising from protons on the phenyl ring, based on correlation between the cyclometalating carbocation peak (vertical axis) and the terminal proton peak (it contains six) located three bonds away.

Experiment: NOESY NMR
This through space experiment allows for definitive assignment of the peaks arising from protons on the benzothiazole ring. One final experiment is required to assign the peaks on the phenyl ring.

Conclusions



The characterization routine established for this complex provides a straightforward method for NMR-based structural determination of complexes belonging to its general class.
Reasons for using this method include:

- Determining definitive peak assignments for the ^{1}H NMR spectrum of a species,
- Verifying that various derivatives have been synthesized as intended, and
- Gathering structural information without the use of X-ray crystallography.

Future work includes:

- Generating a write-up of this characterization method for publication,
- Potentially, repeating this characterization for several similar complexes, and
- Generating a letter-style publication summarizing the results of the solvent optimization project.

Acknowledgments

Thanks to:
Dr. Ryan O'Donnell, Army Research Laboratory
Dr. Thomas (TJ) Rohrabaugh, Army Research Laboratory
Dr. Timothy Cook, State University of New York at Buffalo
Dr. Matthew Crawley, State University of New York at Buffalo
Lauren Rosch, State University of New York at Buffalo

The work conducted this summer was part of an ongoing collaboration with Cook Lab at the State University of New York at Buffalo.

Research was sponsored by the Army Research Laboratory and was accomplished under Cooperative Agreement Number W911NF-20-2-0115. The views and conclusions contained in the document are those of the authors and should not be interpreted as representing the official policies, either expressed or implied, of the Army Research Laboratory or the U.S. Government. The U.S. Government is authorized to reproduce and distribute reprints for Government purposes notwithstanding any copyright notation herein.

University at Buffalo
The State University of New York

cooklab @ub

Online Network Adaptation

Matthew Schack - Colorado School of Mines (mschack@mines.edu)
John Rogers - Army Research Lab (john.g.rogers59.civ@mail.mil)

Motivation

- Communication is important for robotic teams to consider as it allows locally collected information to be distributed to the other team members.
- Communication models computed offline can be inaccurate due to unknown environmental factors---e.g., unseen walls or jamming agents.
- Online models can be more accurate, but also more expensive to compute, hindering their scalability to large environments.
- Our work focuses on a way to adapt a communication model online while partitioning the environment into regions to improve scalability

Previous Work

- (Fink 2013) partitions an environment into regions and learns a linear model for powerloss between regions, improving scalability. However, it requires that the regions be determined by some other algorithm.
- (Twigg 2013) creates a k-means clustering algorithm for grouping space into regions with similar network characteristics. However, the determines the amount of regions based solely on environment size rather than network characteristics.

Method

- We seek to create a network model where the signal strengths recorded (S) between robot positions is within some user defined allowable deviation.

Sampled Strength, Sampled Point

$$|\underbrace{\mathcal{M}(x_1, x_2)}_{\text{Communication model}} - \widehat{c}| \leq \underbrace{d}_{\text{Allowable deviation}} \forall \overbrace{(x_1, x_2, c)}^{\text{Sampled Point}} \in \mathcal{S}$$

- To create this model, we partition the environment into regions, and define a network model between regions (inter-region model) and within regions (intra-region model). If a sampled point doesnt fit a model, we break apart the region.
- **Inter-region model** is defined by linear model similar to (Fink 2013). The model's parameters are found by finding a best fit line from the sampled points.

Sampled Point, Allowable deviation

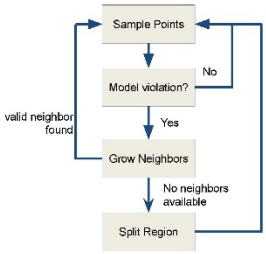
$$\underbrace{a_0 - a_1 \log(||\overbrace{x_1 - x_2}^{\text{Sampled Point}}||)}_{\text{Best fit parameters}} - \underbrace{c}_{\text{Sampled Strength}} \leq \widehat{d} \, \forall (x_1, x_2, c) \in \mathcal{S}$$

- **Intra-region model** has the same constraint as the inter-region model along with a constraint ensuring that the drop in power is always low.

Region

$$a_1 \log(||x_1 - x_2||) \leq \underbrace{\epsilon}_{\text{Small constant}} \forall (x_1, x_2) \in \widehat{\mathcal{R}}$$

- When a pair of points violate either region model, we attempt to add the violators to a neighboring region. If no region can take the neighboring points, then we split the region into two smaller regions.



Acknowledgment

- I would like to thank ARL for the opportunity to participate in meaningful research that will hopefully benefit our armed forces.
- Thank you to Dr. John Rogers for his guidance and help during this project.

Comparison of Cycle-GAN Generated Synthetic Data on YOLO Object Detection

Student: Avik Singh, aviksinghsemail@gmail.com
Mentor: Matthew Thielke, matthew.d.thielke.civ@mail.mil

Abstract

Object detection is an important tool that can be used to track multiple key interests without the need of human intervention. This can be achieved through development and training of Artificial Intelligence systems designed to help users identify and track objects given a large amount of data. The YOLO object detection system (You Only Look Once), is a public repository that allows users to identify objects in an image. Development of such systems requires the AI to train over multiple iterations of object-based images to fully comprehend the object and how to find/track it given new images. The amount of preliminary images required to develop these systems is currently sparse, so a new method of achieving data is necessary. This can be achieved through synthetic data generation. One promising way to generate synthetic data is using Cycle-GANs to transform one type of image into another. Therefore, we can use this to generate IR data given EO data and use that to train YOLO. To test this method's effectiveness, we need to compare this to real world IR data to determine its use cases. Experimentation is needed to find the optimal conversion from EO to IR, but ultimately, this process will help to facilitate our understanding of synthetic data generation.

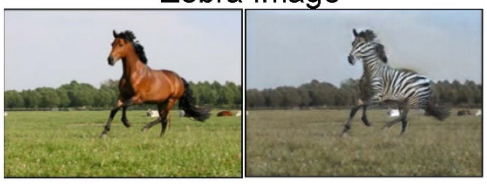
Background

YOLO object detection requires a vast array of images to properly train and test its model, but there is a shortage of the most relevant target datasets that must be addressed. In order to combat this issue, we have looked into the use of Cycle-GAN systems to create synthetic data that enhances the existing datasets for YOLO training. We believe that Cycle-GAN will produce IR data that will improve YOLO detection performance. This project aims to highlight the benefits and costs of using a Cycle-GAN system to generate synthetic data and how it can be used to train YOLO models.

Experiment

In this case, a Cycle-GAN model was created to make horse images look like zebras. Then, a horse image was fed as an input.

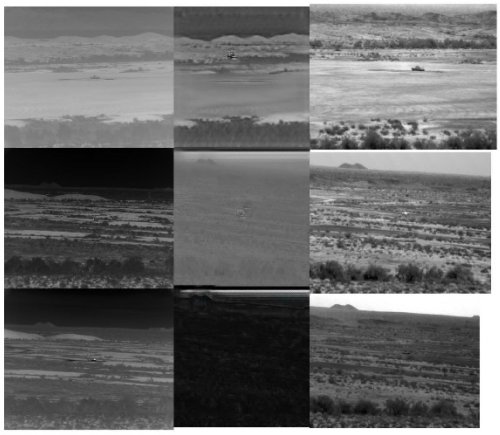
Horse Image
V
Cycle-GAN
V
Zebra Image



Results

From the images below, we can see the result of converting EO data into IR, which shows the data that will be processed by the YOLO object detector. These images were taken from our second iteration of the Cycle-GAN model. During our testing of the YOLO object detection program, we will determine which Cycle-GAN model provided more accurate data for us to use.

Original IR Image Synthetic Data (Fake) Original EO Image



Discussion/Path Forward

To improve upon this project, we can test the validity of using synthetic data by training different Cycle-GAN models with different parameters to generate synthetic data. The YOLO object detector will be trained with synthetic IR data and tested with real IR images to determine the viability of the synthetic data to be used as training data with the YOLO object detectors. Further experimentation is required to answer the following questions:

- What is the scope of data needed to perform well on YOLO?
- What version of YOLO performs the best given CycleGAN data?
- What other types of data (other than IR and EO) can be generated using CycleGAN?

Acknowledgements

- Army Research Lab
- James Uplinger, james.r.uplinger7.ctr@mail.mil
- Cycle-GAN github repo: https://github.com/junyanz/pytorch-CycleGAN-and-pix2pix

UNCLASSIFIED

Information-Directed Reinforcement Learning

Wesley A. Suttle, Ji Liu, Alec Koppel

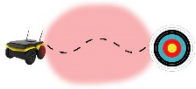
Abstract

In this work we have developed reinforcement learning (RL) algorithms enabling an autonomous agent to minimize cost per unit information acquired about its environment, which we call the information ratio. The information ratio framework can be used to model problems of interest, including patrolling an area of operations (AO) while eliminating targets and "reconnaissance" of an AO while avoiding detection.

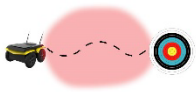
Why Does the Information Ratio Matter?

Example. Imagine a robot learning to find its way to a target in an unknown environment.

- Vanilla policy gradient methods can cause the robot to be **overconfident**, hastily settling on suboptimal or dangerous trajectories.



- Information ratio methods encourage the robot to be **humble**, resulting in cautious, better-informed, more feasible trajectories.



Problem Formulation

- Start with an average-cost Markov decision process $(\mathcal{S}, \mathcal{A}, p, c)$.
- Given parameterized policy π_θ, define:
  - expected average cost: $J(\theta) = \lim_{n\to\infty} \frac{1}{n} \mathbb{E}_{\pi_\theta}\left[\sum_{k=0}^{n-1} c(s_k, a_k)\right]$,
  - entropy measure: $d_\theta(s) = \lim_{n\to\infty} P(s_n = s \mid s_0, \pi_\theta)$,
  - entropy: $H(d_\theta) = -\sum_{s\in\mathcal{S}} d_\theta(s) \log d_\theta(s)$.
- Fix some $\kappa \geq 0$ scaling the importance of information acquisition.
- **Goal:** find policy parameters θ maximizing $\rho(\theta)$.

Information Ratio

$$\rho(\theta) = \frac{J(\theta)}{\kappa \vee H(d_\theta)}$$

Contributions

- Introduced **information ratio** for RL.
- Derived **entropy gradient theorem**.
- Developed **information ratio policy gradient** algorithms and underlying theory.
- Provided promising empirical results.

Theorem 1

Given a policy parameter θ_0, $\nabla_\theta H(d_\theta)|_{\theta=\theta_0} = \mathbb{E}_{s\sim d_{\theta_0}}\left\{-\log d_{\theta_0}(s) - H(d_{\theta_0})\right\} \nabla \log \pi_\theta(a|s)$.

This enables us to empirically sample from $\nabla H(d_\theta)$ and thus $\nabla \rho(\theta)$.

Theorem 2

Given access to the dynamics p and cost c, there exists a concave optimization problem that we can solve to obtain an optimal policy π^* minimizing the information ratio over the MDP $(\mathcal{S}, \mathcal{A}, p, c)$.

Information Ratio vs. Vanilla

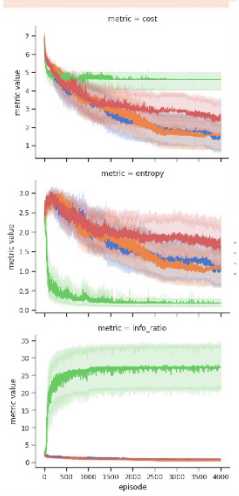


Figure 2: Info ratio actor-critic outperforms vanilla actor-critic on a maze environment. Vanilla actor-critic is actor-critic with $\kappa = 0$, i.e., it does not encourage exploration.

Exploring a Maze

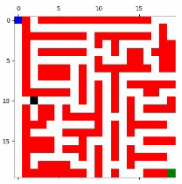


Figure 3: Info ratio actor-critic exploring and solving a maze.

Empirical Results

- Information ratio algorithms find the global optimal solution in the tabular setting.
- Given the same hyperparameters, information ratio actor-critic algorithm far outperforms vanilla actor-critic on an array of different maze problems.

Ongoing Work

- Theoretical convergence analyses of our algorithms.
- Practical information ratio algorithms using neural networks as function approximators.
- Evaluation on simulated reconnaissance and patrol problems.

Contact Information

- Email: wesley.suttle@stonybrook.edu

UNCLASSIFIED

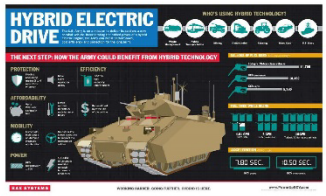
Fast Charging of Lithium-ion Pouch Cells as a Function of Elevated Temperature

ViChi Tran
River Hill High School

ARL Mentor: Dr. Jeff Read
Directorate/Division: SEDD/ES

OVERVIEW

- Future Army applications require a battery with good performance under fast charge rates at high temperatures
- Lithium-ion batteries are good candidates, but to what extent can they perform under a range of temperatures at fast charging rates?



[1]

OBJECTIVES

- Compare two types of li-ion pouch cells and observe their performance at different temperatures under fast charge and then determine the possible source of these differences
- Analyze cycled cells with XRD and SEM to pinpoint the source of any possible capacity fade

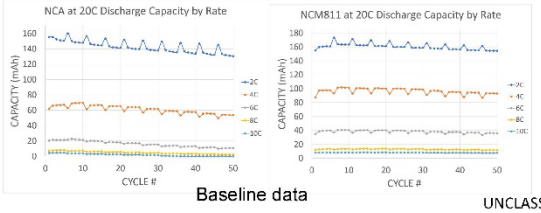




APPROACH

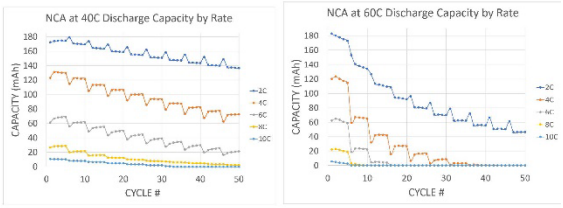
- Prior to cycling, we dried and filled the cells with electrolyte and carried out formation cycling to get baseline performance.
- We tested NCA and NCM811 cells under each set of conditions, collecting data points to determine cell performance.

RESULTS

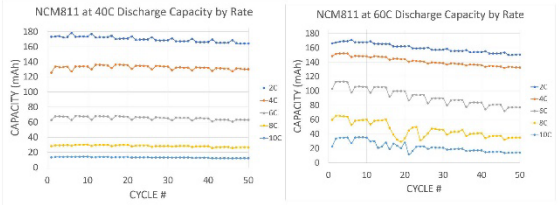


Baseline data

NCA battery capacity quickly deteriorates under faster charge and higher temperatures as shown in the graphs below.



The NCM performance at elevated temperatures is significantly better but shows more deterioration as temperatures increases.



CONCLUSION

- Overall, NCAs cannot withstand higher temperatures without rapidly decreasing in capacity.
- NCMs perform better than NCAs in elevated temperatures, although generally both have much lower capacities at faster charges.

REFERENCES

1. Photo: https://newatlas.com/bae-gcv-hybrid-tank/25113/
2. Ahmed, Shabbir, et al. "Enabling fast charging — A battery technology gap assessment." *Journal of Power Sources*, pp. 250-62. PDF.

ACKNOWLEDGMENTS

I would like to thank Dr. Read for his patience, mentorship, and guidance during this project, and ARL for this opportunity as well.

EVALUATION OF FATIGUE AND WEAR ON ADVANCED MATERIALS IN LOW VISCOSITY FUELS USING REPEATED IMPACTS

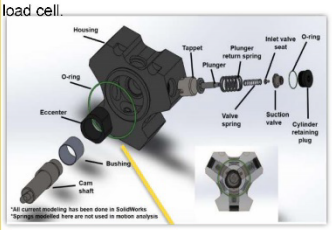
Andrew Velasquez
Master of Science
University of California, Merced

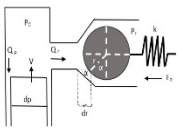
ARL Mentor: Stephen Berkebile
Directorate/Division: CISD/VICTOR ERP
Internship Duration: 06/01/2021 to 08/20/2021

BACKGROUND

High pressure fuel pumps are essential components in air and ground vehicles, but their material compositions vary based on their application. Ground vehicle fuel pumps in the Army are designed for diesel fuels but the Army operates on jet fuels. Lubrication properties of jet and diesel fuels vary, leading to improper lubrication in fuel pumps increasing wear and fatigue in pump components.

Project is continuation of previous approach for failure analysis of check valve system in high pressure fuel pumps. An apparatus was made to simulate ball impacts against orifice in the check valve using a solenoid to drive a steel ball into a solid flat material submerged in jet fuel against a load cell.

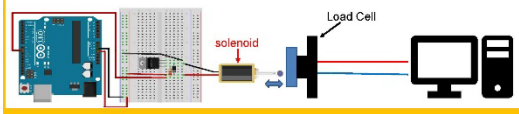




MOTIVATION

Previous impact apparatus had some design problems which made for collecting data from impacts a little difficult. Problems include:

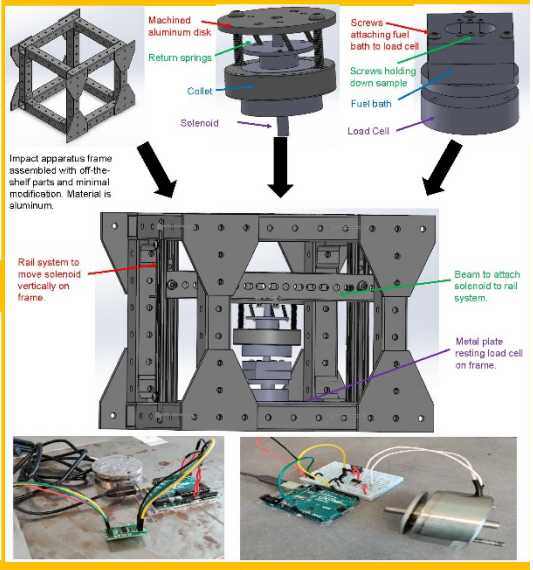
- x Epoxy holding frame joints together becomes unstable in the presence of jet fuel.
- x Holder housing fuel and sample too large requiring unneeded amounts of fuel.
- x Solenoid linear reciprocation inconsistent.



APPROACH

To reduce manufacturing costs for designs, pre-machined aluminum frames were used to make an assembly due to its low machining cost, material price, and corrosive resistance. The method for generating impacts followed the previous method of controlling a solenoid and load cell using a microcontroller. Evaluation of wear on impacted material will be analyzed using optical microscopy and interferometry to view the surface morphology.

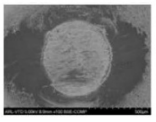
RESULTS

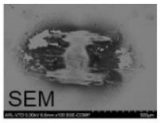


OBJECTIVES

- ✓ Improve the impact apparatus frame for holding solenoid.
- ✓ Design smaller holder to decrease amounts of fuel needed for testing.
- ✓ Generate high cycle fatigue impacts of ball against various materials submerged in fuel.
- ✓ Determine which materials resist abrasive fatigue for longer life cycles in fuels.

F-24 fuel wear scar on ball in air





F-24 fuel wear scar on ball in nitrogen

FUTURE

- ➢ Finish assembling the impact apparatus with solenoid and load cell attached.
- ➢ Test ball impacts against various substrate materials in different jet fuels and other fuel types.
- ➢ Perform post test microscopy analysis on ball and flat material differentiating wear mechanisms towards failure.
- ➢ Make table of material combination impacts and determine which ones resulted in less wear.

REFERENCES

Aidan. "Controlling a Solenoid with an Arduino" et al. Fuel Processing Technology 129 (2015).
Agarwal et al. Fuel 105 (2013).
Arkoudeas et al. Fuel Processing Technology 122 (2014).
inc - Tutorial." *Core Electronics*, 22 Nov. 2018. core-electronics.com.au/tutorials/solenoid-control-with-arduino.html.

ACKNOWLEDGEMENTS

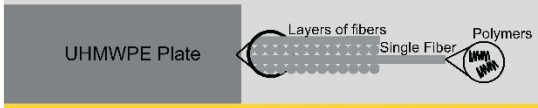
Ashlie Martini, Monica Ferrona, Kevin Kannar, David Gundel

Developing a Property Linked, Parameter Driven Model of UHMWPE Plate Material

Travis Wagner, BS/MS Mechanical Engineering
Mentor: Dr. Richard Becker
WMRD-Physics of Soldier Protection ERP

Introduction

Ultra High Molecular Weight Polyethylene (UHMWPE) plate material is a highly anisotropic composite used in various armor applications. The material comprises of two main parts, the UHMWPE fibers, and the matrix within which these fibers are constrained. The material is highly modifiable, mainly by changing the fibers, the matrix, and the consolidation process. The goal of this project is to further the development of a model, which has input parameters that are linked to the physical properties of the material. This will allow the model to both predict experimental performance and suggest change in the manufacturing process.

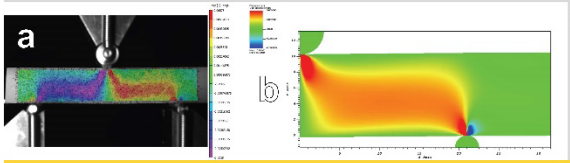


Left: A schematic showing the hierarchy of UHMWPE material makeup.
Right: An image showing the alignment of the fibers in UHMWPE plate material. The matrix would be present between the fibers in the voids.



Modeling UHMWPE Fiber Composites

Modeling each fiber and matrix layer explicitly is limited by computation, therefore a homogenized material model is used to represent multiple layers at once. This homogenized material model represents the contributions the fibers and the matrix have in the mechanical behavior, along with other mechanisms present between the two materials. Properties of single fibers are well known and can be entered, along with bulk properties of the solid. The response of the composite under combined loading yields the most difficulty, with multiple mechanisms governing the response in different regions. The model was fit to the load response and strain contours of short beam shear and three point bending experiments. Modeling two similar experiments with different geometries tests for robustness that cannot be determined from a single experiment. Below, the experimental and simulated contours can be compared. Note the angles of the strain bands, and the off-centered nature of the main band, which was matched by modifying the material model.



(a) The experimental short beam shear strain contour of Tensylon HS.
(b) The strain contour of the simulated Tensylon short beam shear, using the updated continuum model. The model was modified and fit to achieve this response.

Adding Mechanisms to the Model

The model was changed to add a different fiber modulus that becomes active under compression, which is being validated by ongoing experiments. The model was also edited to include a strain hardening effect into the slip mechanism. The compressive modulus was added to capture the yield stress difference between the short beam and three-point experiments. Slip hardening was added to adjust the contour geometry.

Acknowledgements

Special thanks to Dr. Richard Becker, Dr. Daniel O'Brein, Dr. Christopher Hoppel, Dr. Andrew Tonge

Effects of Dodecane Soaking Time on Friction Performance and Wear on Stainless Steels

Harry Wise

Motivation

- Current Army fuel pumps experience ***wear at metal interfaces***
- Lubrication by low viscosity fuel = main cause
- Better understanding of tribological interactions and surface phenomena between steels and fuels → ***better component performance***

Methodology

- Measure baseline friction coefficient with n-dodecane on 52100 and D2 steels
- Determine friction coefficient reduction via experimental matrix:

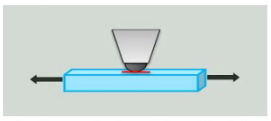
Trial/Soak Time	0 hrs	0.5 hrs	3 hrs	15 hrs	24 hrs
1	0.296	0.0469	0.073	0.105	0.147
2		0.207	0.127	0.178	
3					

Standard Sample Parameters:

Vickers Hardness	374 ± 18 HV0.3
Avg. Surface Roughness, R_q	20.2 ± 2.7 nm

Tribological Conditions:

Vertical Load	2 N
Frequency	5 Hz
Duration	1 hr



Tribometer diagram showing relative motion between ball (gray) and sample (blue)

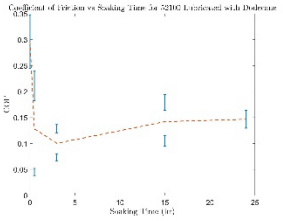
Post-test processing:

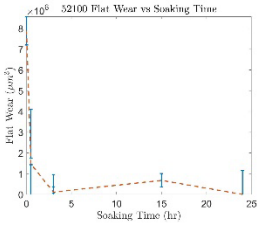
- ***Raman spectroscopy*** to detect tribofilm formation on ball
- ***Confocal microscopy*** to determine wear volume of ball and sample

Goal & Hypothesis

- **Goal:** Determine the soak time effect on friction coefficient of dodecane fuel
- **Hypothesis:** Increasing soak time causes reproducible decrease in friction coefficient due to increased adsorption of molecules to surface

Results





- COF is reduced significantly within first 3 hours of soak time
- Extended soak times (15 and 24 hours) increase COF slightly
- Wear volume on ball and sample reduces with soak time; consistent with COF

Next Steps

- Complete 3 tests per soak time for better statistics
- Complete tribotesting matrix of 52100 and dodecane
- Select 2 or 3 soak times that lead to the best friction performance and test under varying temperatures
- Standardize grind orientation to increase reproducibility

Acknowledgements

- Dr. Q. Jane Wang, Dr. Y.H. Chung, Dr. Stephen Berkebile
- Tobias Martin, Ph.D student

Heart Rate Synchrony using MDRQA

Julie Young
Univ. of Maryland, CP
Data Science and Applied Math

Mentors:
Greg Gremillion, Brandon Perelman
HRED HAT ERP Office

Project Goal

The goal of this project is to:

- Evaluate team states through real-time physiological measures to inform team reconfiguration
- Measure biological synchrony by performing MDRQA on heart rate of dyadic operators pairs

Background

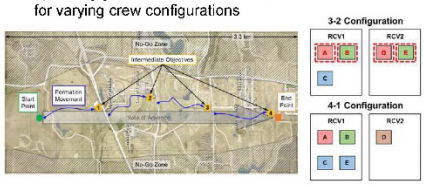
Coordination patterns between multiple physiological signals over time indicate teamwork[2]

Trust building activities have been shown to correlate to greater physiological recurrence between dyad partners than in dyads that do not engage in trust building[3]

Expect higher physiological synchrony (recurrence) in dyads performing coordinated tasks (building trust)

Methodology

Utilized previously collected pre-pilot test data of crews operating ground vehicles in simulated combat mission for varying crew configurations



Captured measures of ECG waveform, interbeat interval, respiration waveform, and 3-axis accelerometry from lightweight wearable wireless sensor belt (Zephyr BioHarness)



Analysis

Compare recurrence metrics of matched dyads (gunners and drivers) within a vehicle to unmatched dyads in different vehicles to evaluate physiological synchrony

Multidimensional Recurrence Quantification Analysis (MDRQA) is a recurrence-based analysis that measures synchrony within signals Utilized open-source MDRQA algorithm [4] that provides:

- Recurrence Plot – visual representation of recurrence
- Recurrence Metrics – statistical information including percentage of recurring points, determinism, percentage of diagonally recurrent points and percentage of vertically adjacent points, along with standard statistical measures (i.e. mean, max, min)

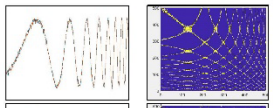
References

1. J.S. Shockley, M. Riley, J.J. Zbilut, C.L. Webber, Cross recurrence quantification of coupled oscillators, *Phys. Lett. A* 305 (2002) 59–69.
2. J.M. Marwan, N. Wessel, U. Meyerfeldt, A. Schirdewan, J. Kurths, Recurrence-plot-based measures of complexity and their application to heart-rate-variability data, *Phys. Rev. E* 66 (2) (2002) 026702.
3. Mitkidis, P., McGraw, J. J., Roepstorff, A., & Wallot, S. (2015). Building trust: Heart rate synchrony and arousal during joint action increased by public goods game. *Physiology & Behavior, 149*, 101–106. https://doi.org/10.1016/j.physbeh.2015.05.033
4. Wallot, S., Roepstorff, A., & Mønster, D. (2016). Multidimensional Recurrence Quantification Analysis (MdRQA) for the Analysis of Multidimensional Time-Series: A Software Implementation in MATLAB and Its Application to Group-Level Data in Joint Action. *Frontiers in Psychology*, 7. https://doi.org/10.3389/fpsyg.2016.01835

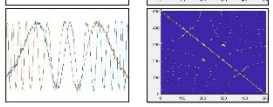
Results

Test cases: signals being evaluated (left) and recurrence plot (right)

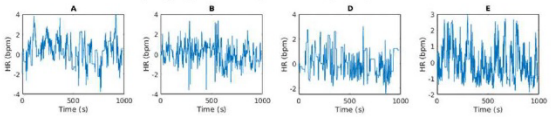
Synchronous (high recurrence) signals



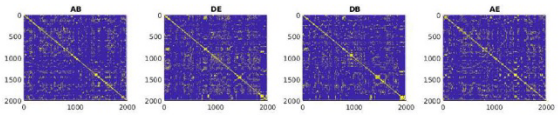
Asynchronous (low recurrence) signals



Heart rate (HR) signals for operators A, B, D, and E



Recurrent plots for match pairs (AB and DE) and unmatched pairs (DB and AE)



Recurrence metrics for each pairing

	AB	DE	DB	AE
Recurrence (%)	0.97	1.06	1.01	1.05
Diagonal Adjacency (%)	50.3	53.0	57.1	53.1
Mean Length (Diagonal)	2.50	2.43	2.91	2.54
Max Length (Diagonal)	16	20	43	46
Vertical Adjacency (%)	79.0	84.2	80.6	83.9
Mean Length (Vertical)	2.95	2.77	3.60	2.84
Max Length (Vertical)	19	22	51	47

Recurrence plots and metrics did not indicate a trend of higher synchrony in HR signals of matched dyad partners as compared to unmatched operators

May be due to limited quantity of highly noisy data and limited variation in trust and teamwork during interactions

Future Work

Evaluate recurrence metrics on other physiological modalities and for moving windows of smaller time intervals

Compare recurrence metrics against self-report measures of teamwork and team trust

Perform analysis on human subjects data with greater data quality and quantity

Further my experience in working with data and learning different types of analysis

Acknowledgements

Alex Danvers
Sean Fitzhugh
Joe Rexwinkle
Jonroy Canady
David Chhan

OPTIMAL CONFIGURATIONS FOR FLOATING GATE TRANSISTORS

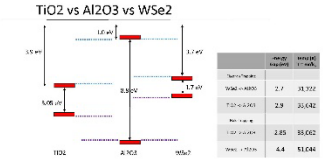
Zuri Rashad, Hampton University – DoD Researcher, zurirashad@gmail.com
Mentor: Dr. Sina Najmaei, DEVCOM ARL ALC (Adelphi, MD)

Motivation/Objective

- There is a need for transistors in computers to be made smaller and with greater memory capacity.
- Floating gate devices combine a logic and memory component within a single transistor to operate memory and logic simultaneously.
- Finding semiconductor materials with a wide variation in electron band gaps will allow the floating gate device to have a charged trap effect.

Rationale

- A semiconductor (WSe_2), barrier oxide (Al_2O_3), and tunneling oxide (TiO_2) are stacked from top to bottom while being placed atop a doped substrate and connected to a voltage source.
- When the power source is on, the electrons should have enough energy to jump to the conduction band (blue) and when powered off the electrons move down to the valence band (purple).



Results

Semiconductor to Barrier Oxide	Thickness (nm)	Voltage Applied (V)	Current Density (A/nm²)
$WSe_2 \rightarrow Al_2O_3$	0.1-2.0	0.1-2.0	0-400
$WSe_2 \rightarrow HfO_2$	0.1-2.0	0.1-2.0	0-400
$WSe_2 \rightarrow Si_3N_4$	0.1-2.0	0.1-2.0	0-400

Discussion/Conclusion

- Using the Fowler-Nordheim Tunneling equation, the current density was calculated for barrier oxides with a width between 0.1-2.0nm, and a voltage input between 0.1-2.0 V.
- A high current density indicates that the barrier oxide can trap charged electrons even when the device is powered off, indicating that the floating gate device has non-volatile memory properties.

$$J = \frac{q^3 E^2}{8\pi h q \phi_B} \exp\left[\frac{-8\pi(2qm_T^*)^{1/2}}{3hE}\phi_B^{3/2}\right],$$

Pathway Forward

- The goal is to simulate the range in current densities using as many semiconducting materials as possible, including titanium oxide, aluminum oxide, tungsten selenide, hafnium oxide, and silicon nitrate.
- Studying the configurations with different tunneling methods, such as direct tunneling and Schottky emissions, will also provide a more accurate prediction on the current density within the device.
- The strongest results will lead to building a prototype in the laboratory will provide the best estimation of voltage outputs from the floating gate device.

Acknowledgements

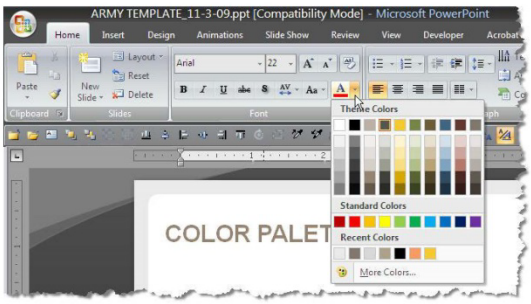
- A Review on Conduction Mechanisms in Dielectric Films (Fu-Chien Chiu, Ming Chuan University)
- Hampton University Department of Defense STEM Scholarship
- Army Research Laboratory, Adelphi Lab Center, Sensors and Electron Devices Directorate, Advanced Electronics Division

HAMPTON UNIVERSITY

UNCLASSIFIED

UNCLASSIFIED

Each template has its own color palette. It is the top row of colors under the "Font Color," "Shape Fill" and "Shape Outline" menus





UNCLASSIFIED

1 (PDF)	DEFENSE TECHNICAL INFORMATION CTR DTIC OCA
1 (PDF)	DEVCOM ARL RDRL DCL TECH LIB
2 (PDF)	DEVCOM ARL FCDD RLL PP P COLLINS D DIGGS